AD-A286 632

FAULT DETECTION TECHNIQUES FOR COMPLEX CABLE SHIELD TOPOLOGIES

Kurt H. Coonrod
Stuart L. Davis
Donald P. McLemore

Kaman Sciences Corporation
6400 Uptown Blvd, NE
Albuquerque, NM 87110

September 1994

Final Report

DTIC
ELECTE
OCT 2 0 1994
S
G
D

94-32644

PHILLIPS LABORATORY
Advanced Weapons & Survivability Directorate
AIR FORCE MATERIEL COMMAND
KIRTLAND AIR FORCE BASE, NM 87117-5776

94 10 19 067

PL-TR--93-1111

This final report was prepared by Kaman Sciences Corporation, Albuquerque, New Mexico, under Contract F29601-92-C-0109, Job Order 3763AHNA with the Phillips Laboratory, Kirtland Air Force Base, New Mexico. The Laboratory Project Officer-in-Charge was William D. Prather (WSR).

This report has been reviewed and is approved for publication.

WILLIAM D. PRATHER, GM-14
Project Officer

FOR THE COMMANDER

DANIEL T. McGRATH
Major, USAF
Deputy Chief, EM Sources Division

WILLIAM L. BAKER, GM-15
Acting Director, Advanced Weapons and
Survivability Directorate

REPORT DOCUMENTATION PAGE

1. AGENCY USE ONLY (Leave blank)	2. REPORT DATE September 1994	3. REPORT TYPE AND DATES COVERED Final 24 Aug 92 – 24 Aug 93

4. TITLE AND SUBTITLE

FAULT DETECTION TECHNIQUES FOR COMPLEX
CABLE SHIELD TOPOLOGIES

6. AUTHOR(S)
Kurt H. Coonrod, Stuart L. Davis, and
Donald P. McLemore

5. FUNDING NUMBERS

C: F29601-92-C-0109
PE: 64711F
PR: 3763
TA: AH
WU: NA

7. PERFORMING ORGANIZATION NAME(S) AND ADDRESS(ES)

Kaman Sciences Corporation
6400 Uptown Blvd, NE
Albuquerque, NM 87110

8. PERFORMING ORGANIZATION REPORT NUMBER

9. SPONSORING/MONITORING AGENCY NAME(S) AND ADDRESS(ES)

Phillips Laboratory
Kirtland AFB, NM 87117-5776

10. SPONSORING/MONITORING AGENCY REPORT NUMBER

PL-TR—93-1111

11. SUPPLEMENTARY NOTES

12a. DISTRIBUTION / AVAILABILITY STATEMENT

Approved for public release; distribution is unlimited.

12b. DISTRIBUTION CODE

13. ABSTRACT (Maximum 200 words)

This document presents the results of a basic principles study which investigated technical approaches for developing fault detection techniques for use on cables with complex shielding topologies. The study was limited to those approaches which could realistically be implemented on a fielded cable, i.e., approaches which would require partial disassembly of a cable were not pursued. The general approach used was to start with present transfer impedance measurement techniques and modify their use to achieve the best possible measurement range. An alternative test approach, similar to a sniffer type test, was also investigates.

14. SUBJECT TERMS
Fault Detection, Shield Cable Tester (SCT), Transfer Impedance
Meter (TIM)

15. NUMBER OF PAGES
66

16. PRICE CODE

17. SECURITY CLASSIFICATION OF REPORT Unclassified	18. SECURITY CLASSIFICATION OF THIS PAGE Unclassified	19. SECURITY CLASSIFICATION OF ABSTRACT Unclassified	20. LIMITATION OF ABSTRACT SAR

CONTENTS

By _____
Distribution /

Availability Codes	
Dist	Avail and / or Special
A-1	

iii

FIGURES

FIGURES (CONCL.)

1.0 INTRODUCTION

This document presents the results of a basic principles study which investigated technical approaches for developing fault detection techniques for use on cables with complex shielding topologies. The study was limited to those approaches which could realistically be implemented on a fielded cable, i.e., approaches which would require partial disassembly of a cable were not pursued. The general approach used was to start with present transfer impedance measurement techniques and modify their use to achieve the best possible measurement range. An alternative test approach, similar to a sniffer type test, was also investigated.

1.1   BACKGROUND

There is a requirement for mission critical systems on most military equipment to be hardened to the effects of Electromagnetic Pulse (EMP), Electromagnetic Interference (EMI) and lightning. A common way of achieving this is to enclose all electronics in a continuous shield. The weak link in this type of design is the use of shielded cables to interconnect the line replacement units (LRUs) of the system. These cables are very susceptible to degradations, or faults, over time. To maintain adequate shield integrity on these cables requires periodic inspection, testing and repair.

The Shielded Cable Tester (SCT) was the first test instrument developed to measure the shielding performance of cables "as-installed" on an aircraft. This capability is important because it provides a convenient and cost-effective method for finding shield degradations and assessing the need for repair. The SCT also provides a high fidelity technique for determining the life cycle behavior of shielded cables. The Transfer Impedance Meter (TIM) was developed to miniaturize and package the SCT's functionality in a truly portable test instrument.

In some cases where the SCT and TIM have been used, particularly on the aircraft, situations have arisen where these testers have not detected what was considered an obvious fault. This problem has typically occurred on cables with complex shield geometries (i.e., cables with multiple layers of shield overbraid and/or internal shields

from twisted shielded pairs, triaxial or coaxial inner conductors). The theoretical transfer impedance of these cables is below the nominal sensitivity of the SCT and TIM. The fact that visibly degraded cables have not resulted in a corresponding measured degradation has raised questions about the ability of the SCT and TIM to detect hardness critical faults in these types of cables. The hardness impact of these faults needs to be assessed, and new test techniques may need to be developed to better evaluate these types of cables.

1.2 PURPOSE

The purpose of this task is to research basic test techniques which may be used in evaluating cables with complex shield topologies. In doing this, this task will also address the general relationship between test capabilities (instrumentation limitations), shielding provided by complex shield topologies and the shielding requirements of systems.

1.3 DOCUMENT ORGANIZATION

As background, Section 2.0 provides a list of documents which are applicable to the present test effort. A description of the mockup cable to be used in the experiments is presented in Section 3.0. Section 4.0 presents the results of the investigation of different test techniques. Section 5.0 presents the results of a characterization of the sample cable in both baseline and faulted conditions. Section 6.0 presents a summary of the results and recommends a procedure to be followed when measuring these types of cables.

2.0 RELATED DOCUMENTS

Many important concepts used in this effort have been previously documented. The companion report "SCT - TIM Cable Testing Protocol"* contains the general procedures for testing cables in situ using the SCT and TIM, a description of the "trace wire" concept, and fault isolation techniques. This document also presents a brief discussion of transfer impedance, which is the physical quantity that best describes the level of protection provided by cable shielding, and is the quantity measured by the SCT and TIM.

The "TIM1 Versus Rack Mounted SCT Report,"** documents detailed laboratory experiments to determine the precision and accuracy of each instrument, along with measurement comparisons between the two instruments made on both stable test samples in a controlled laboratory environment and on fielded cables tested at a depot.

---

*   Coonrod, Kurt H., Jurisson, Karl R., and J. Todd Hendrickson, (TRW, Albuquerque Engineering Office), TIM—SCT Cable Testing Protocol, Kaman Sciences Corporation Report No. DC-TR-2216.301-5, May 1993. To be published as Phillips Laboratory Report No. PL-TR-93-1110.

**   Davis, Stuart L. and Kurt H. Coonrod, TIM1 Versus Rack Mounted SCT Report, TRW, Albuquerque Engineering Office Report No. 58773-A002UT-00, October 1, 1992.

3.0 COMPLEX CABLE DESCRIPTION

Thorough evaluation of possible test techniques requires a stable set of pristine and faulted cable samples. Cable degradations (and even new cables), however, are sensitive to handling, and the transfer impedance of a cable assembly actually changes when the cable is flexed and connectors are re-mated. The changes should be small (less than a milliohm) for new cables, but the contact impedance in corroded joints and coupling through small holes can change dramatically when the test sample is disturbed. These considerations led to the need for a stable laboratory quality mockup of the complex cable shielding topologies that could have representative and repeatable faults introduced and removed as required during the test technique evaluation.

Several aircraft cables with complex shield topologies were examined in order to determine the requirements for the cable mockup. The most complex topology was used as the basis for the design of the mockup cable. This cable consisted of 19 individual triaxial cables surrounded by a triple layer of outer shielding. The three layer overbraid was constructed using two layers of standard flexible shield overbraid with a layer of copper foil sandwiched in between. The triaxial cables had their outer shields terminated via pigtails to the connector backshell. The inner shield and the core of the triaxes were attached to coaxial pins which were mounted in the connector.

The test cable was built following this same design. Figure 1 shows a breakout drawing of the cable. The numbers on the figure will be referenced in the description that follows. A 30-in-long section of the triple overbraid was formed around a plastic tube (8). At one end of the cable the braid (8) was pulled over a solid brass cylinder (9) which is threaded at the other end. This in turn screws into a copper radio frequency (RF) box (10) where inner shield and core wire terminations are made. The other end of the test cable mates to a similar cylinder (7) except that it is in two pieces which clamp together like a clam shell. This allows intentional faults to be inserted into the overbraid by changing out pieces of the cylinder. A 50% circumferential fault is added by replacing one of the brass halves of the cylinder with a dielectric half. A 1/2-in long slit fault is inserted by replacing a solid half of the cylinder with a brass piece with the slit in it.

straight plug

box mount
receptacle
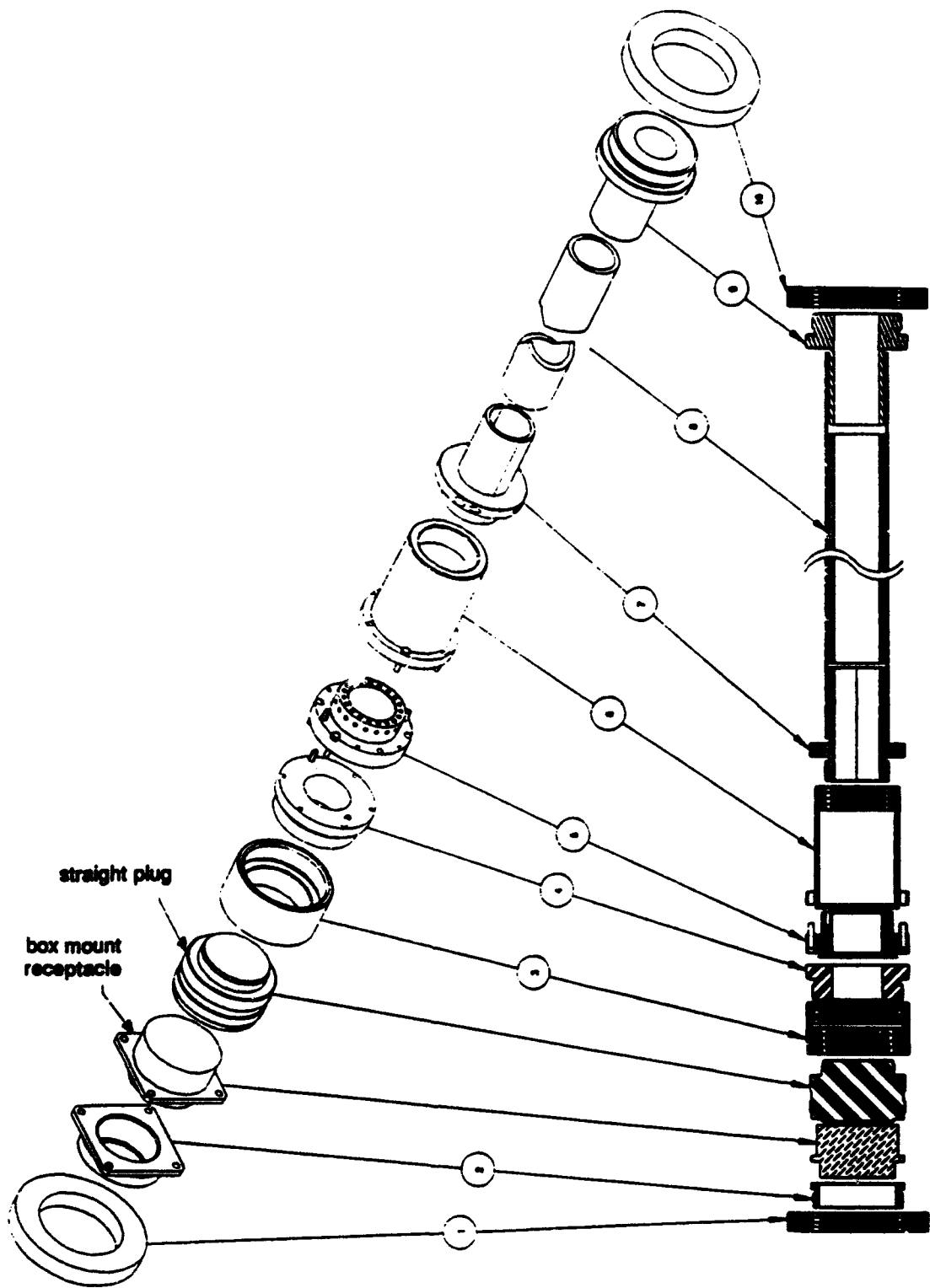
Figure 1. Breakout drawing of the test cable.

5

The two piece cylinder is then threaded into a solid brass cylinder (6) which simulates a connector backshell. This piece covers the inner cabling where the triax pigtails are split out. This solid cylinder is then attached via four screws and RF gasketing to a brass fitting (5) which simulates the tag ring in a real connector. This is where the outer shields of the inner triaxial cables are terminated. The tag ring is attached at the other side via four screws and RF gasketing to a threaded brass fitting (4) which mates to another copper RF box (1). An optional mating connector pair can be inserted into this joint by using two brass adapters (2 and 3). The second copper box contains all the instrumentation interfaces for measuring coupling to the inner wiring.

Faults to simulate joint corrosion can be installed either before or after the tag ring. These faults are constructed from two thin brass rings with a phenolic ring sandwiched in between and fifty chip resistors soldered across the gap. When installed between (5) and (6), these faults act on the triple overbraid only. When installed between (4) and (5), these faults also act on the outer shield of the triaxial cables.

Several triaxial cables and a single trace wire were fed through the overbraided plastic tube. At the far end of the cable the outer shields of the triax cables were terminated via pigtails to ground inside the termination copper box. The length of these pigtails was a little longer than was seen on the sample aircraft cable. The inner shield and the core wires of the triax were shorted together and the two were terminated inside the copper box. At the near end of the cable, the outer shields of the triax cables were terminated via pigtails to the overbraid at the tag ring. The inner shields and core wires of the triaxes were fed through to the interface copper box and attached to coaxial pins which could be either grounded, left floating or instrumented. Figure 2 shows a cross section of the test cable shielding topology.

These shield layers are
joined at the connector for
each triax

Outer layer
of overbraid

Outer shield
of triax

Copper
foil

Inner shield
of triax

Inner layer
of overbraid

Pin of triax

Suggested
trace wire
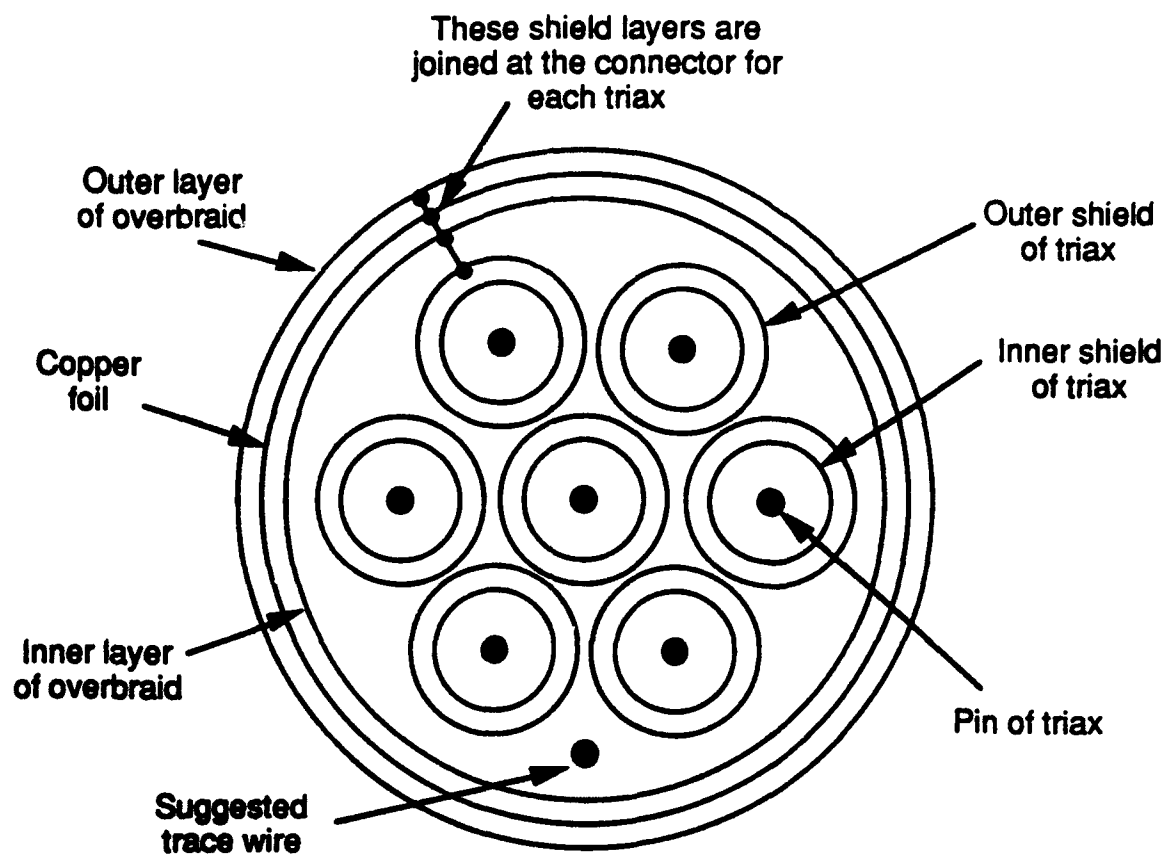
Figure 2. Test cable shielding topology.

4.0 TEST TECHNIQUE INVESTIGATION

Cable transfer impedance is a fairly simple concept – the voltage induced on a core wire per unit current on the shield – and although different measurement techniques may have certain advantages in particular situations, they are all based on driving a known current on the shield and measuring a voltage induced on an internal wire. Since the heavily shielded aircraft cables have very small transfer impedances and the faults apparently do not significantly increase the transfer impedance, the concentration was on ways to improve the dynamic range (or lower the noise floor) of the present test techniques.

4.1   CONTINUOUS WAVE

A wide dynamic range can be achieved with relatively straightforward CW test techniques. The SCT is a swept CW technique that uses an HP 3577 network analyzer to drive current on the cable shield and simultaneously measure the induced voltage on a core wire. Figure 3 shows the standard SCT test setup. In this setup, a current probe inductively couples up to 100 mA onto the cable shield, and since the network analyzer can easily measure voltages in the microvolt (μV) range, dynamic ranges of 100 dB are easily achieved. Previous evaluations of the standard SCT setup (the Mk-21 W5A1 SCT, built for SAALC) have shown that it can detect the end-to-end d.c. resistance of the cable (R_{dc}) values on the order of 4 $\mu\Omega$ and M_{12} values on the order of 75 pH.

Methods for improving the dynamic range and sensitivity of the basic SCT setup were investigated. These included increasing the shield current, amplifying the measured core voltage, averaging several measurements, and ways to mitigate the influence of the instrumentation cables. Some of these approaches are also applicable to the TIM. The TIM, which is a stepped CW tester, will be discussed in Section 4.1.6.

Since the copper foil in the mockup provides 100% optical coverage, there should be no inductive component for the baseline configuration. A basic philosophy used in these investigations, then, was to be very skeptical about "apparent" inductances and contact resistances beyond the skin-depth roll-off. Iterative experiments were performed, modifying the test setup to isolate and eliminate these contaminations.

This process worked well in an earlier test of a solid copper conduit. Documentation of this earlier test is instructive, and it is included as the Appendix.
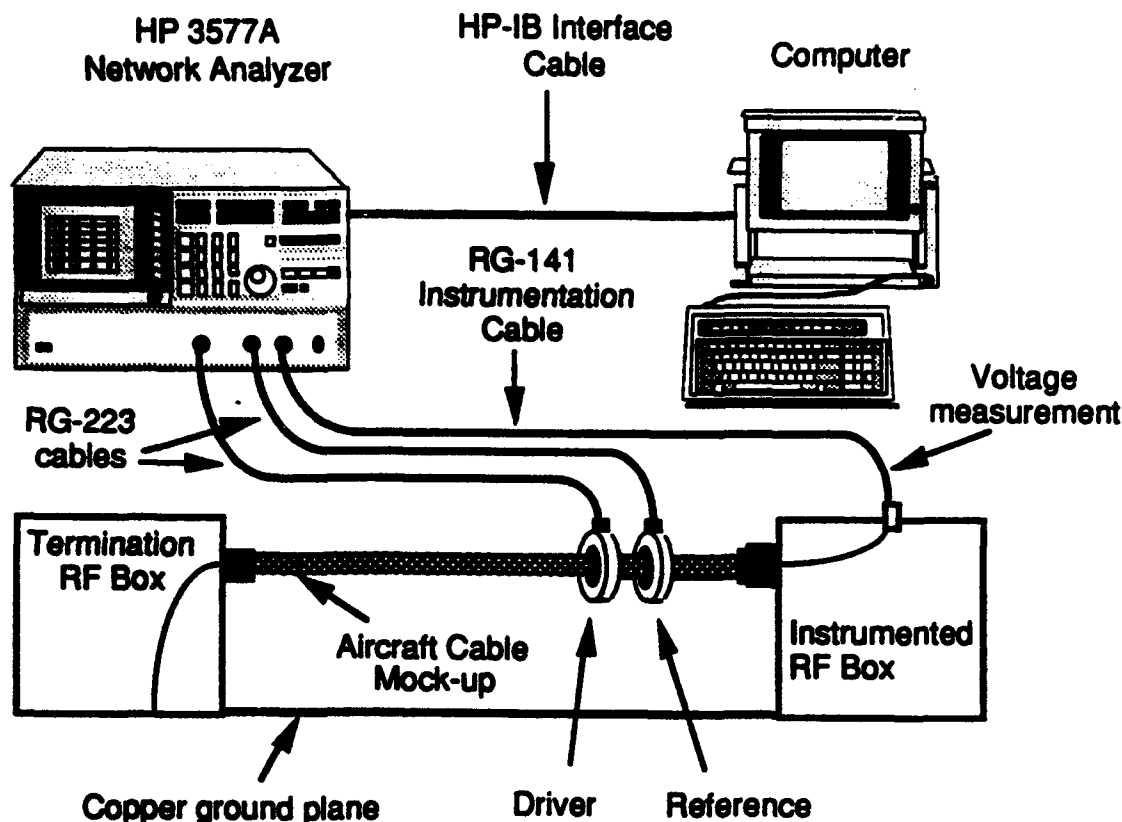
Figure 3. Standard SCT test setup.

4.1.1 Boosting the Drive Current

By increasing the shield current by some factor K while the noise floor on the voltage measurement remains constant, the signal to noise ratio should be improved by the same factor K. In this experiment a 250-W wideband power amplifier increased the current, as shown in Figure 4. The output of the amplifier had to be held a little below maximum because of supply power constraints (the building circuit breakers could not handle the load). Ideally it should have been possible to put a peak current of 1.3 A on the test cable but the limit was just under 1 A.
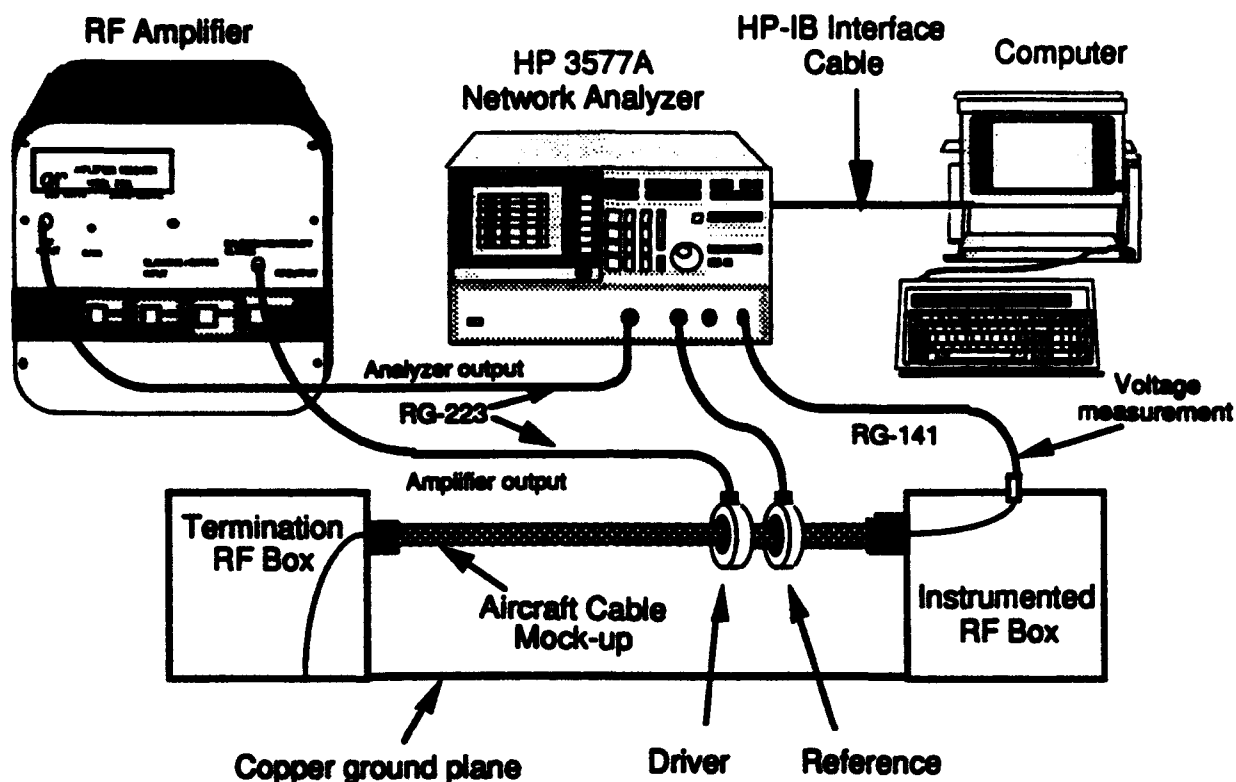
Figure 4. Test setup when using power amplifier.

Figure 5 shows the shield current with and without the power amplifier (the plot legends indicate the file names of the raw data). An improvement was expected in the signal to noise ratio of about 20 dB. Figure 6 shows an overlay of a baseline transfer impedance measurement of the cable mockup with and without the power amplifier. As can be seen there was an improvement in the signal to noise ratio. However in the mid-frequency area around 2 MHz it appears that there was cross coupling between the amplifier and the network analyzer. This reduced the effective improvement in the signal to noise ratio.
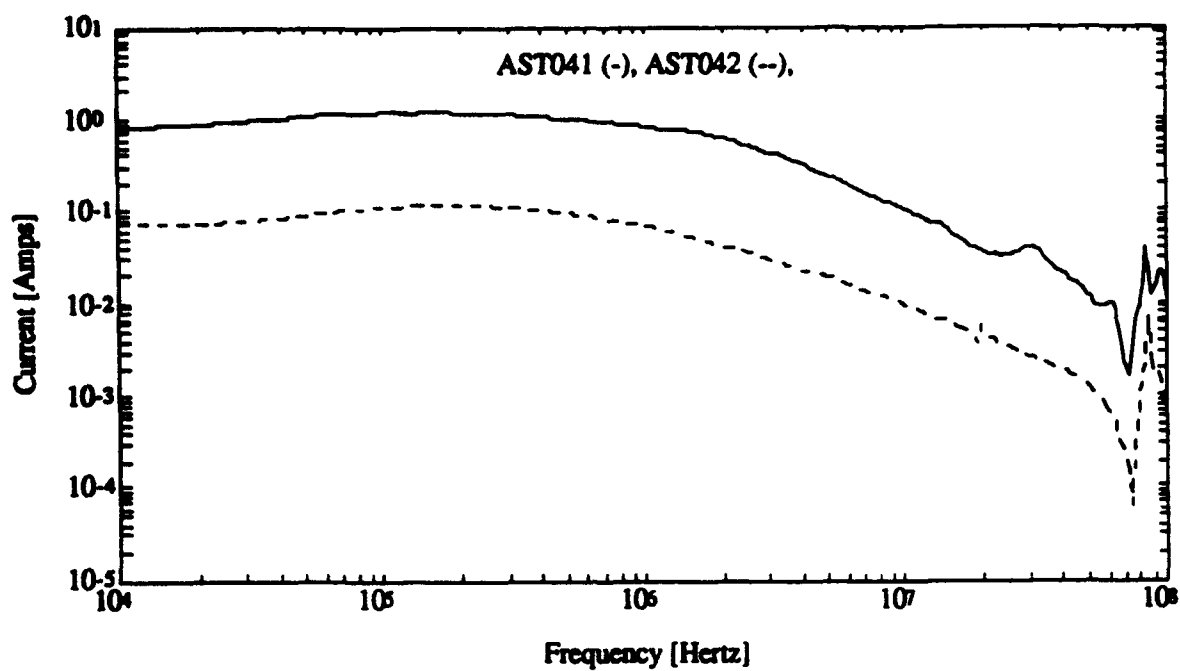
Figure 5. Shield current unamplified (AST042), and amplified (AST041).
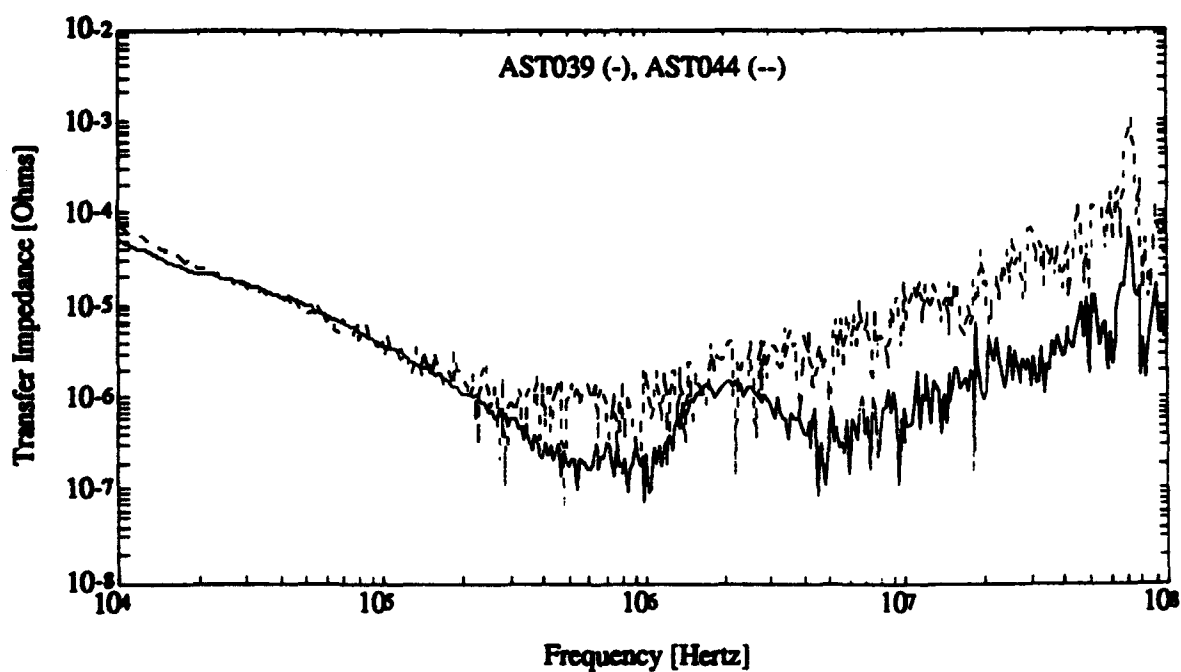
Figure 6. Baseline measurement unamplified (AST044) and amplified (AST039).

11

Through a limited effort, the source of the cross coupling was unable to be isolated and eliminated. Note that the "baseline" plots shown in these examples are for comparison of each proposed technique and do not necessarily depict an optimal baseline measurement. For reference, the rising noise floor at high frequencies should allow detection of inductances as low as 0.02 pH.

Amplification of the shield current is potentially a useful way to increase the dynamic range of the basic SCT setup. This technique is best suited for a controlled laboratory environment and is not very practical for a field test situation. The equipment is cumbersome and the danger of RF burns are a concern.

4.1.2   Averaging the Measurement

A repetitive signal contaminated with random noise can be averaged over many samples and the noise reduced by the square root of the number of samples. The network analyzer produces a very repeatable signal and it has the capability to internally average a measurement up to 256 times. This should reduce the noise by a factor of 16 times, thus improving the signal to noise ratio by 24 dB.

Figure 7 shows an overlay of a baseline measurement using a triax core wire for the sense when only one measurement was made and when 256 averages were taken. It can be seen that the noise was reduced by about 24 dB. The drawback to this approach is time. Considering a standard 10-s SCT sweep speed, it would take about 45 minutes to average 256 sweeps. Note that halving the number of averages (and therefore cutting the time to 23 minutes) should reduce the noise by 21 dB.

This technique works well and it is also best suited for the laboratory environment. In the relatively uncontrolled field environment it may be difficult to maintain an unperturbed test setup for the long periods required (although it has certainly been done for globally swept CW testing), and it may be impractical to tie up an aircraft for the time required to measure all the important cables.
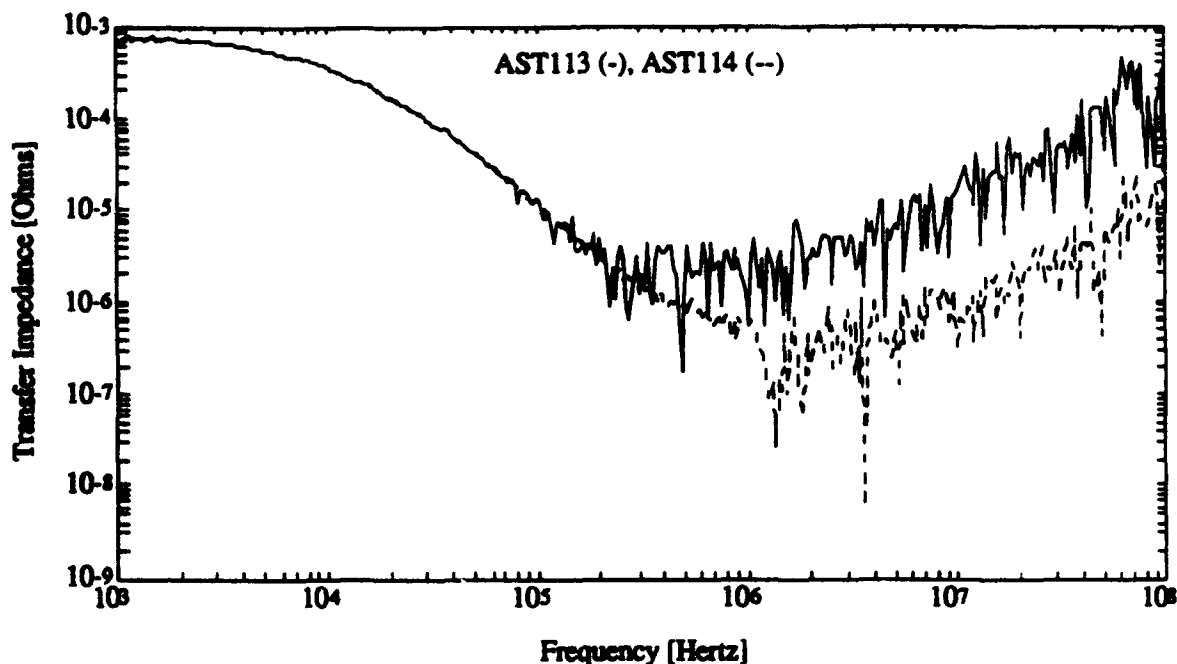
Figure 7. Baseline measurement with one measurement
(AST113) and averaged 256 times (AST114).

4.1.3   Instrumentation Cable Shielding

When making an SCT measurement, ideally the current should just be driven in a loop
over the test cable. However, at higher frequencies this does not happen. The current
begins to couple to the sense voltage instrumentation cable which attaches the
interface box to the network analyzer. This is described as the bleed-back current. As
frequency increases a greater portion of the drive current couples to this path.
Figure 8 shows an overlay of test cable current and instrumentation cable current for
the standard test setup.

When current is coupled to the instrumentation cable it becomes part of the total
measurement. The measured voltage now equals the current on the test cable times
its transfer impedance plus the current on the instrumentation cable times the
instrumentation cable's transfer impedance. When measuring cables with very small
transfer impedances the quality of the instrumentation cable becomes critical. If the
cable being measured is 10 times better than the instrumentation cable and one tenth

of the drive current couples to the instrumentation cable then there is an equal voltage contribution from both the test and instrumentation cable.

Typically RG-223, a double overbraid coaxial cable which is generally considered to be a good cable is used in SCT setups. However, when measuring cables with very low transfer impedances RG-223 is not good enough. Figure 9 shows a transfer impedance overlay of the test cable with all layers of shielding included first using RG-223 as the instrumentation cable on channel A and then using semi-rigid RG-141 with ferrite beads. It is obvious that at the higher frequencies the instrumentation cable dominates the measured response. When these same two measurements are averaged 256 times the data corruption becomes even more obvious as is shown in Figure 10.
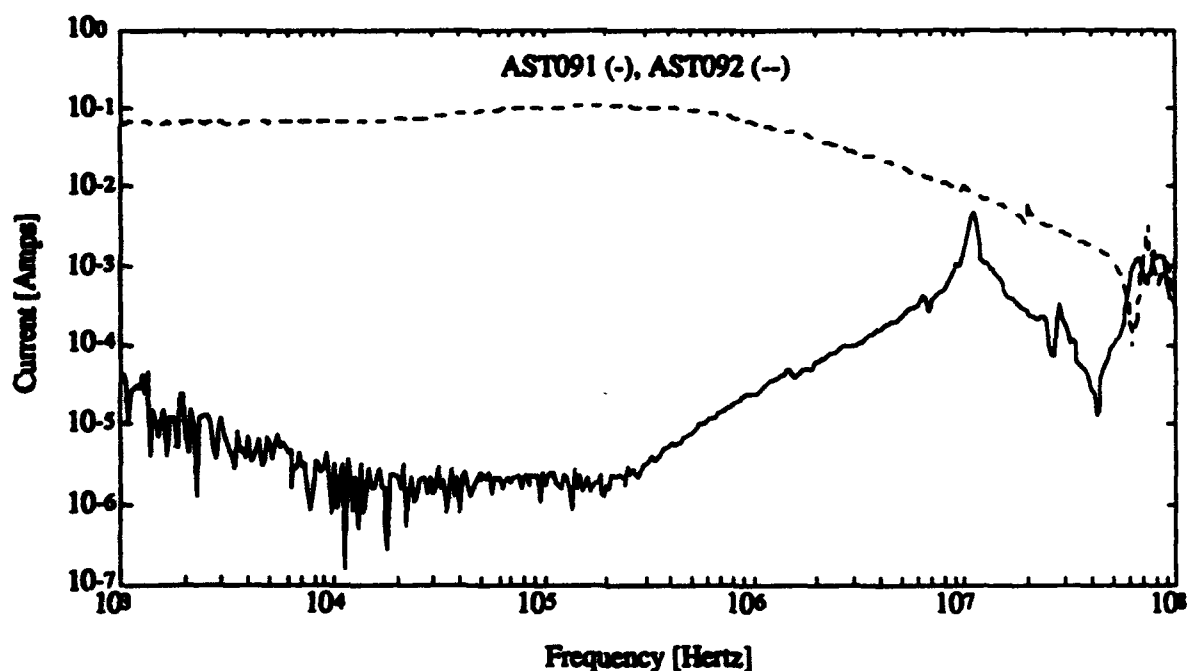
Figure 8. Current coupled to the test cable (AST092) and coupled to the voltage instrumentation cable (AST 091).

14
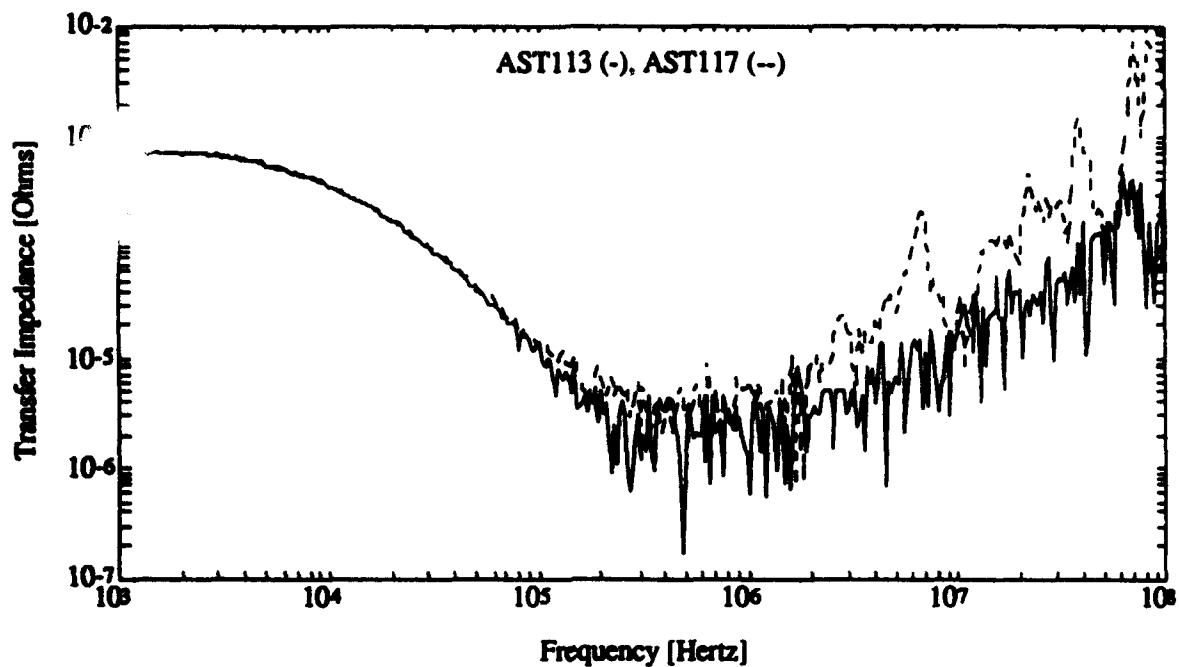
Figure 9. Baseline response of test cable using RG-223 as instrumentation cable (AST 117) and using semi-rigid RG-141 (AST 113).
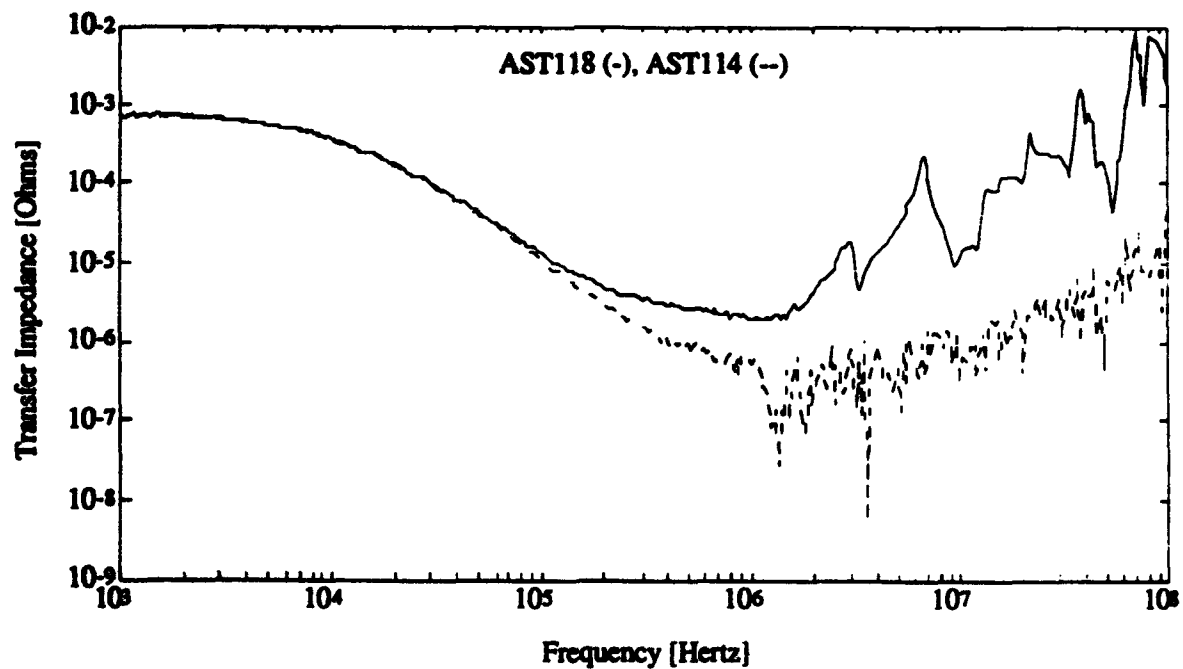
Figure 10. Baseline response of test cable using RG-223 as instrumentation cable (AST118) and using semi-rigid RG-141 (AST114), data averaged 256 times.

The experiment performed here used a 10-ft-long piece of RG-223. When the SCT is used in the field this cable can be as long as 50 ft. The bleed back coupling to this length of cable is probably greater. In a laboratory environment it is very simple to improve the instrumentation shielding by using RG-141. However, when testing is done in the field it is not very practical. Other forms of isolation such as fiber optics may be more practical for field use.

4.1.4   Amplifying the Voltage Measurement

Another approach to increasing the signal to noise ratio of the measurement system is to amplify the measured signal before external coupling can contaminate it. This approach was investigated by placing a wideband instrumentation amplifier directly on the interface box. This amplifier was a three stage AC coupled Avantek amplifier package with 42 dB of gain. The gain of the amplifier was measured and folded into all measurements.

A measurement of the baseline setup was made without the amplifier and then with it. The amplifier measurement had large resonances above 3 MHz which was thought to be caused by coupling with the power supply. To get around this, a battery was used to power the amplifier and the data were re-taken. Figure 11 shows an overlay of the measurement without the amplifier, with the amplifier powered by a power supply and with the amplifier powered with a battery. This figure shows that using the amplifier actually introduced coupling to the measurement channel, making the noise floor worse. The reason for this is that at the higher frequencies the signal being amplified was smaller than the internal noise floor of the amplifier.

There was no benefit to using these particular amplifiers on channel A. To see an improvement would require an amplifier that is sensitive in the nanovolt range. The TIM input amplifiers are not this sensitive, and neither is the network analyzer input. There was no search for other amplifiers beyond the Avantek models.

16
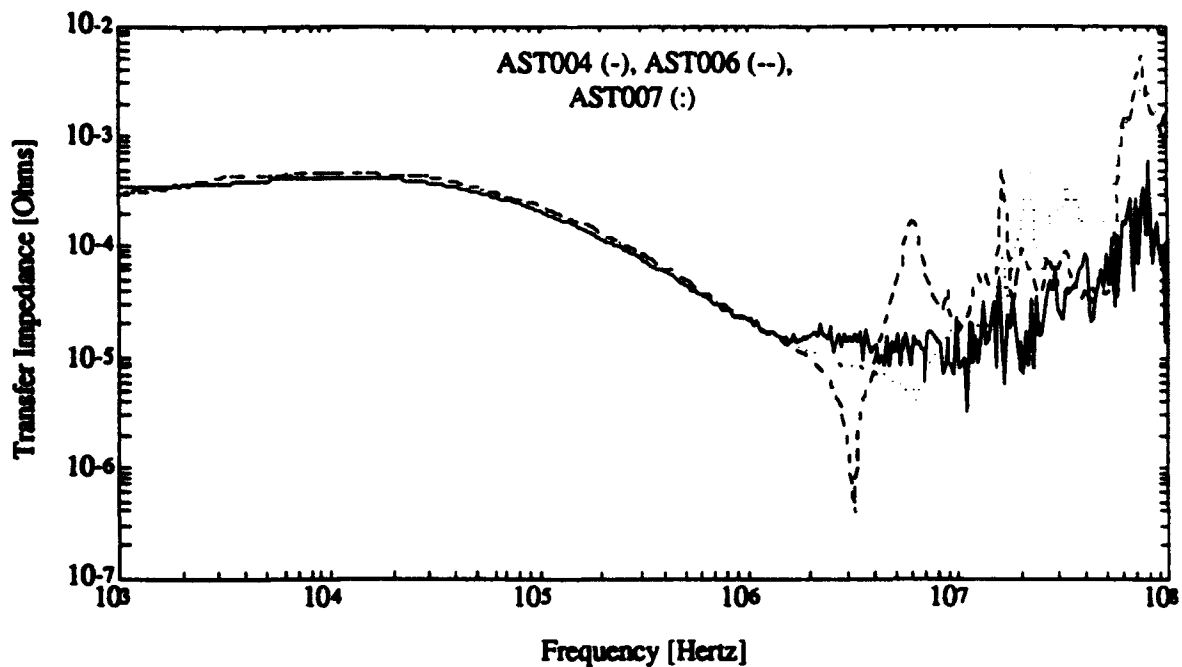
Figure 11. Baseline response, without amplifier(AST004), with amplifier powered with power supply (AST006) and with amplifier powered with a battery.

4.1.5 Sniffer Test

A totally different approach was injecting a signal on one of the core conductors of the cable and detecting leakage with an antenna and spectrum analyzer. The experiments were quite limited with little being done to optimize the receiving antenna configuration. The basic setup was to use the network analyzer as the source, amplify the output with the power amplifier and drive a core conductor in the cable and measure any leakage through the shield using a biconical antenna attached to the spectrum analyzer.

First, with the drive circuit off, a measurement was made of the background emissions. Then the cable was driven and a new measurement was taken. The network and spectrum analyzer were set up to sweep overlapping frequencies, the signal was swept many times and the peak responses captured. These data were then compared to the ambient measurement to see if any leak was detectable. If leakage was detected, then the network analyzer was tuned to that frequency to focus on that area.

17

The antenna was then moved around the cable to obtain the peak reading, which occurred at the source of the leakage. Using this technique it was possible to locate large faults.

4.1.6   Techniques Applicable to the TIM

Most of the techniques discussed above could be applied to the basic TIM test setup. The one area that is not really a problem for the TIM at present is the influence of the instrumentation cable (assuming a mating connector adapter is used instead of the specialized Transfer Impedance Probe). This is because the TIM samples at frequencies where bleed-back coupling is not a large concern.

The easiest technique to implement for the TIM would be amplification of the drive current. This could be done using an external, separately powered amplifier. Since the TIM drives at a limited number of discrete frequencies, a more practical amplifier than the large wideband amplifier may be feasible (perhaps a custom built battery powered unit).

A more drastic TIM modification would be to enhance the amplifier circuit for the voltage measurement. The TIM already provides about 80 dB of voltage signal gain, and any additional amplification would require additional power and a larger case. This is a feasible modification, but as described above the amplifier would have to have a sensitivity in the nanovolt range. The input sensitivity requirement could be relaxed if the drive current were first increased. Note, however, that additional input amplifiers would require more space and power, which would make the instrument more cumbersome to use on an aircraft, and size and weight was a critical design issue for the TIM.

By modifying the TIM code, we could take advantage of averaging the signal many times to reduce the noise floor. The TIM already does this in a limited sense (it compares five quick measurements to ensure steady contact is made, and if the results vary too much the TIM reports "a noisy signal" error condition). This additional averaging, however, would first require a stronger voltage signal (the amplification described above) to be fed into the A/D converters within the TIM unit.

4.2   PULSE EXPERIMENTS

Using a pulse test approach was only briefly investigated because it became obvious quite early on that CW techniques had much more dynamic range. Experiments were performed using the Analogic waveform generator and a high level pulser setup. Because of the expected signal to noise limitations the test setup was modified to only include the overbraid layers of the test cable.

The pulse experiments did not have enough sensitivity to accurately determine the shielding quality or small faults. The programmable waveform generator, however, because of its high fidelity output and ability to interface via the IEEE 488 bus, allowed pulse detection of larger faults using a relatively low level signal. The CW techniques were far superior in dynamic range, and the pulse data are presented in detail primarily as an interesting documentation of the difference between the two techniques.

4.2.1   Analogic Waveform Generator

The baseline cable CW measurement on the "overbraid only" configuration, using standard SCT techniques is shown in Figure 12. This was a clean measurement, well within the dynamic range of the network analyzer. In the region of interest, from 1 MHz to 10 MHz, the current inductively driven on the shield was about 10 mA, and the coupled voltage of about 0.5 μV, giving a transfer impedance of about 50 $\mu\Omega$.

Consider the typical EMP waveform coupled to a cable shield in an aircraft - a damped sinusoid of a few amperes at a few megahertz. The Analogic programmable waveform generator was used in a direct drive test setup (Figure 13) to simulate this coupling. The Analogic was able to drive about 60 mA on the shield, with the waveform shown below (in the time, Figure 14 and frequency, Figure 15 domain, and note that the late time high frequencies have been filtered via a "segmented processing" routine).

19
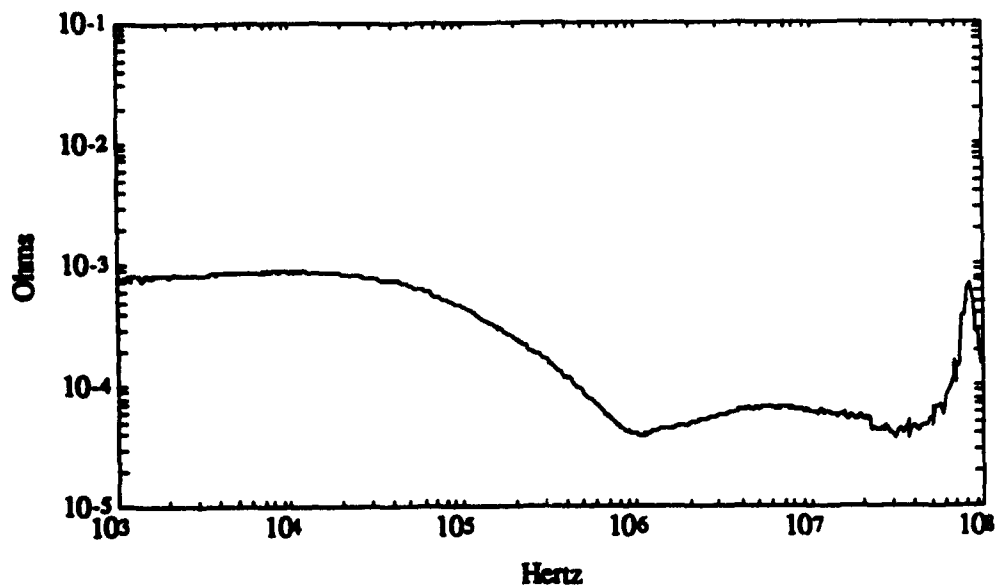
Figure 12. Transfer impedance of the test cable overbraid.
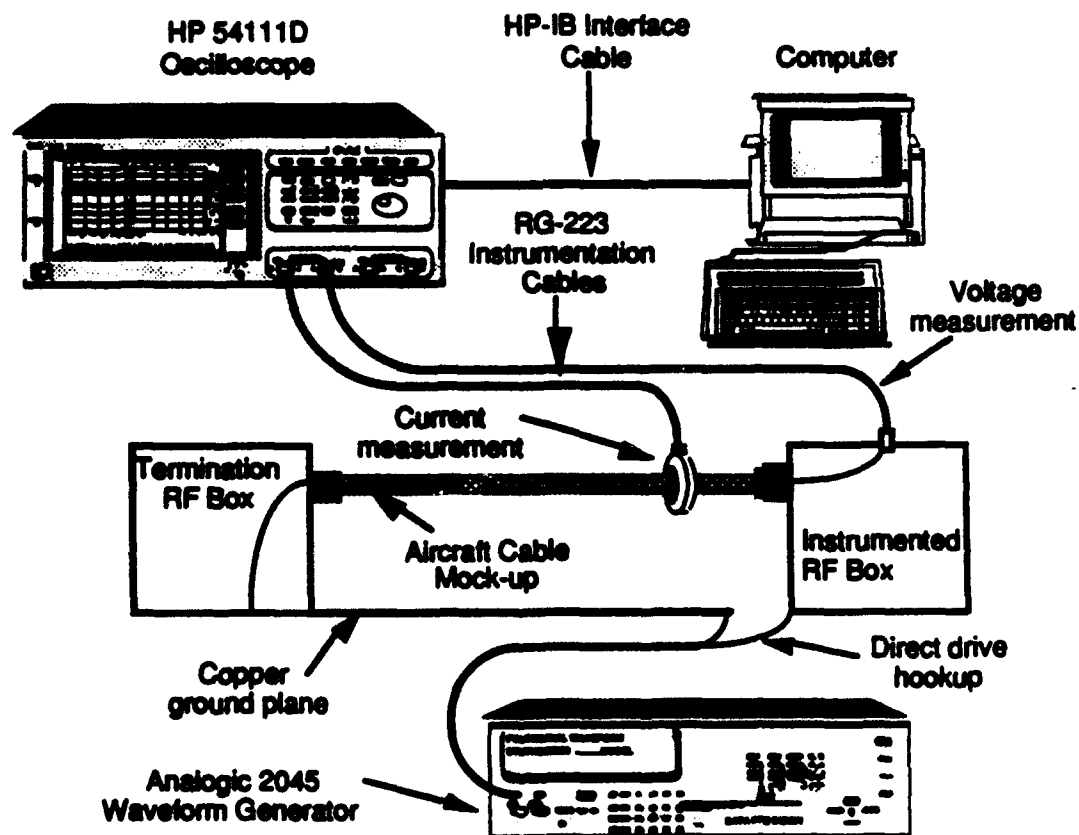
Figure 13. Test setup using the Analogic to direct drive the cable shield.
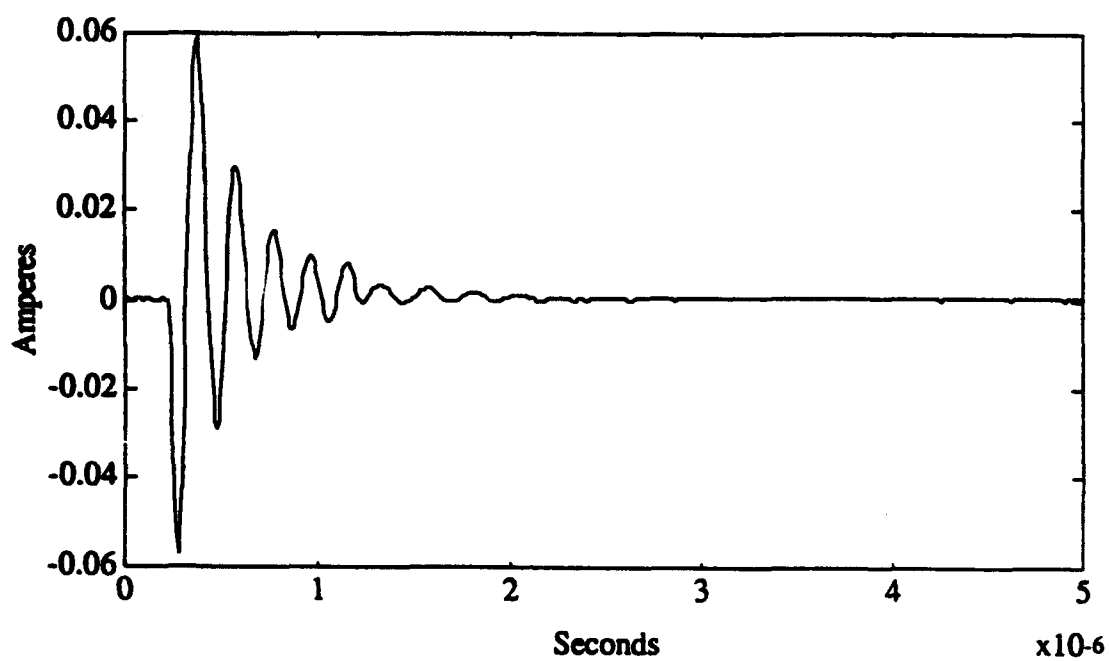
Figure 14. Waveform coupled to overbraid.
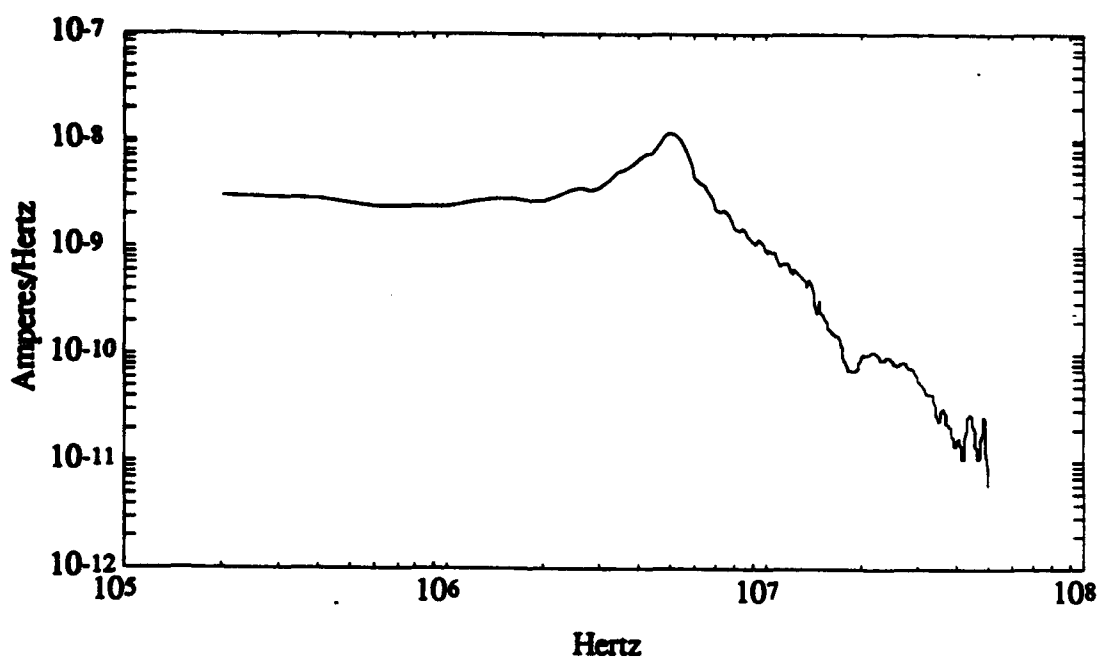
Figure 15. Frequency domain of shield current.

Using simple arithmetic, the peak core voltage developed from transfer impedance coupling would be expected to be only about 3 μV (60 mA times 50 $\mu\Omega$). This is much less than can be measured using the digital oscilloscope (at the scope's most sensitive setting of 1 mV per division, the digitized amplitude bins are about 30 μV apart). The expected voltage waveform can be generated on the computer (by multiplying transfer impedance by the drive current in the frequency domain and then converting back to the time domain), and this computed waveform is shown in Figure 16.
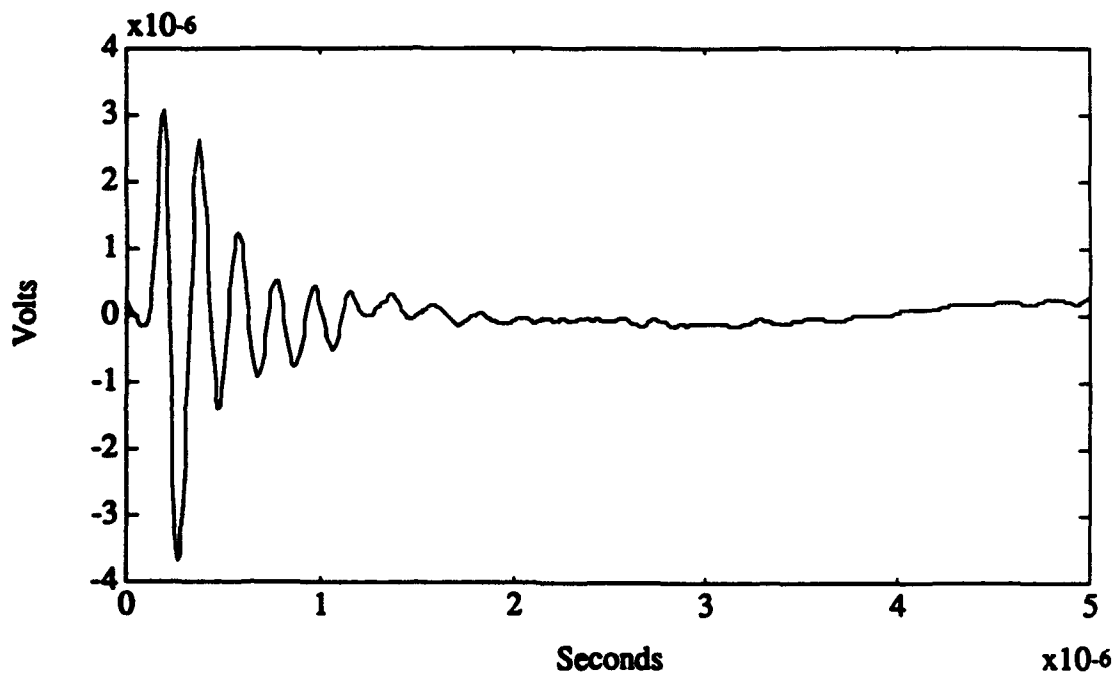
Figure 16. Predicted core voltage coupled from Analogic direct drive.

Figure 17 is the actual voltage on the oscilloscope from this drive. measured from measured waveform. The expected waveform (from Figure 16) is definitely obscured by the digital noise.
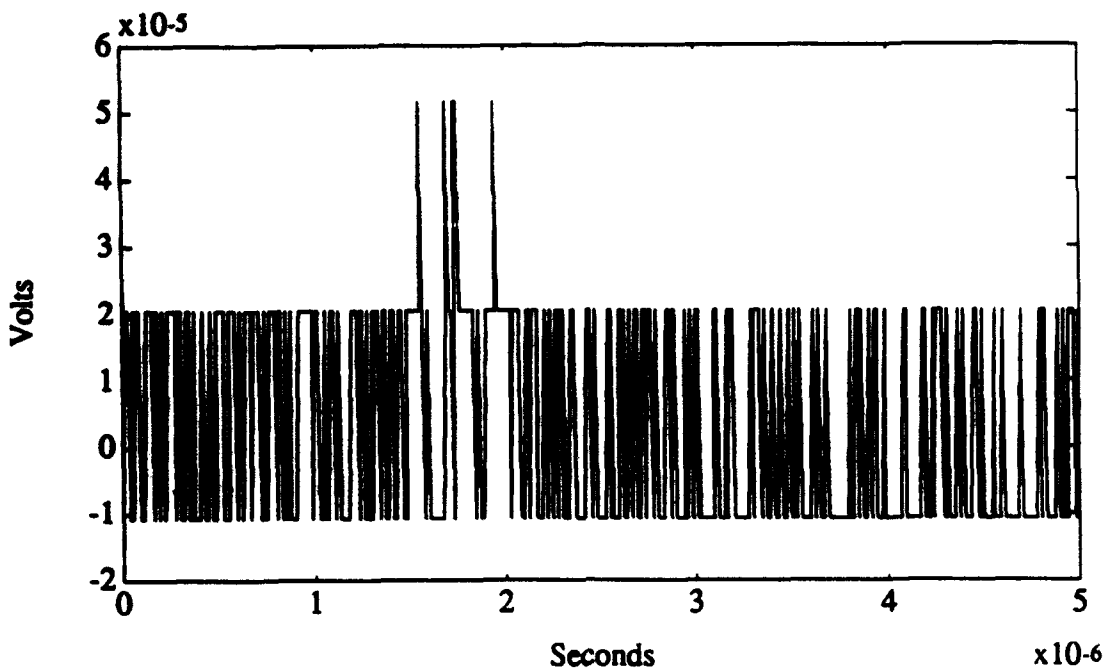
Figure 17. Actual baseline core voltage measured with an oscilloscope.

With such a low transfer impedance, a large shield current would be required to generate any significant core voltage. For example, the largest currents seen on aircraft cables, about 100 A (10 A is actually a more realistic value), would produce only about 5 mV. It would take an unrealistic shield current (20 kA) to produce a voltage as large as the typical LRU box strength specification for a sensitive box (10 V).

Could the core voltage be measured driving the Analogic with the RF amplifier? The amplifier is 500X bigger than Analogic $(5V)^2/50\Omega = 0.5$ W. The RF amplifier is 250 W, so 500X. Since current increase goes as the square root of the power increase, there would be 22.3X more current with the RF amplifier. Since there is 60 mA peak current with Analogic alone, there would be 1.3 A with the Analogic and the RF amplifier. Since the predicted peak voltage from the Analogic drive is 3 µV, the RF amp would couple 67 µV peak to the core in a baseline condition. With about 30 µV per sample point, this is only 2 sample points zero to peak. The core voltage is still in the noise floor of the digital oscilloscope, even when driven by the RF amplifier. Add the triaxial cables and tie their outer shields together at the connector joint and the coupled voltage would be even smaller.

The bottom line for the baseline shielding case is that pulse techniques will not have adequate sensitivity to obtain an accurate measurement of the shielding. A CW technique, with a very low noise floor, is required to see the small coupled voltages. This does not mean, however, that a fault could not be seen with a pulse technique.

With a 50% circumferential fault, (remember that this is the overbraid only, and the scenarios that are about to be described do not apply when the triaxial cables are installed because there is additional shielding and current sharing) the net transfer impedance may be large enough to measure the voltage coupled to the core wire. Figure 18 shows an SCT measurement of the "overbraid only" configuration with a 50% circumferential fault installed. The inductance of the fault is ≈0.6 nH (note that the transfer impedance of the cable actually continues upward with the 20 dB per decade trend, and that the null at about 60 MHz is due to the test setup.
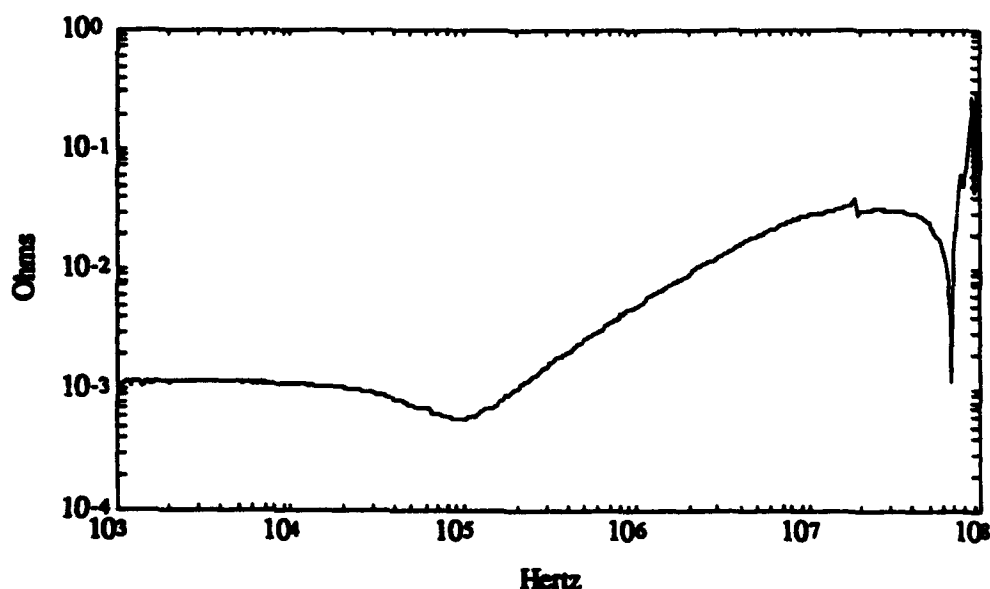
Figure 18. Overbraid transfer impedance with 50% circumferential fault.

Using the example frequency of 5 MHz, the inductance of the fault represents a 20-mΩ transfer impedance. Then the 60 mA Analogic drive would produce about 1 mV on the core wire. Figure 19 shows a time domain measurement of the coupled voltage on the core wire, and Figure 20 shows these data in the frequency domain (these data have also undergone "segmented processing" to remove late time high frequencies).
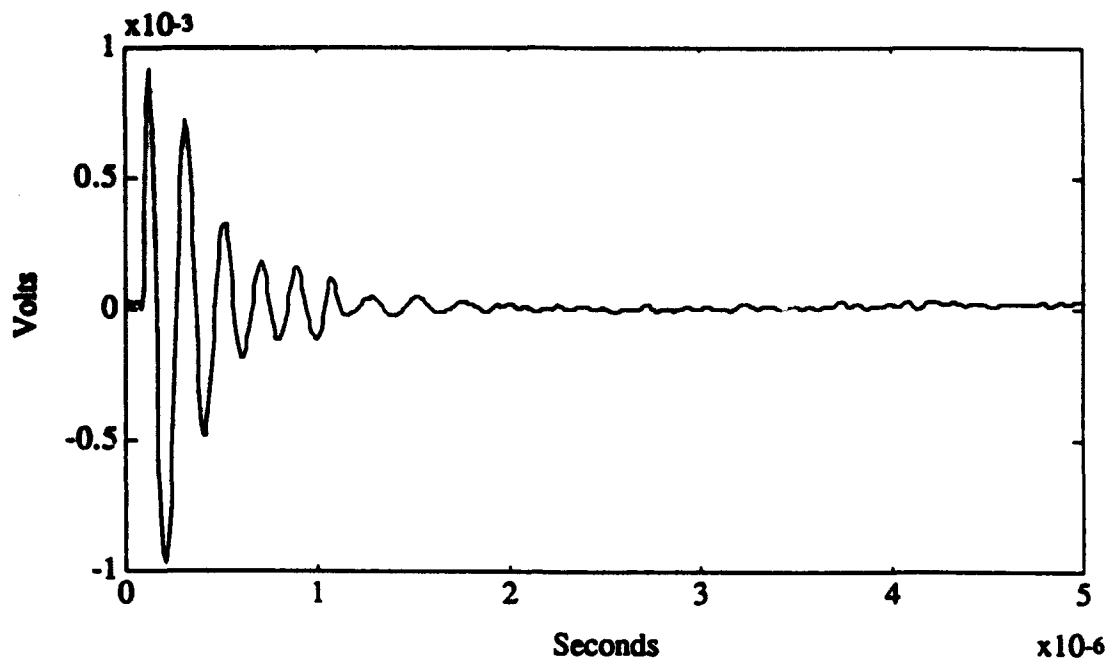
Figure 19. Voltage measurement with 50% circumferential fault.
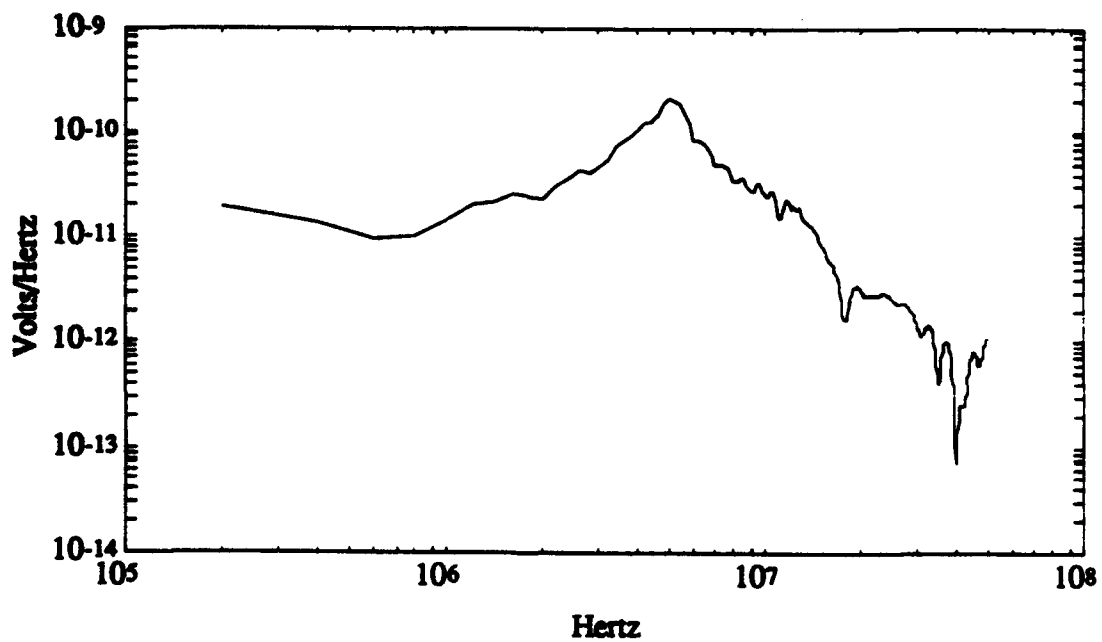
Figure 20. Core voltage measurement in the frequency domain.

In this case the measured peak is very close to the arithmetically predicted peak. Figure 21 shows the predicted waveform generated by multiplying the frequency domain shield current by the transfer impedance and then calculating the inverse transform. This looks very close, so now look at an overlay (Figure 22): the time bases and offsets have been matched, but the amplitudes have not been modified.
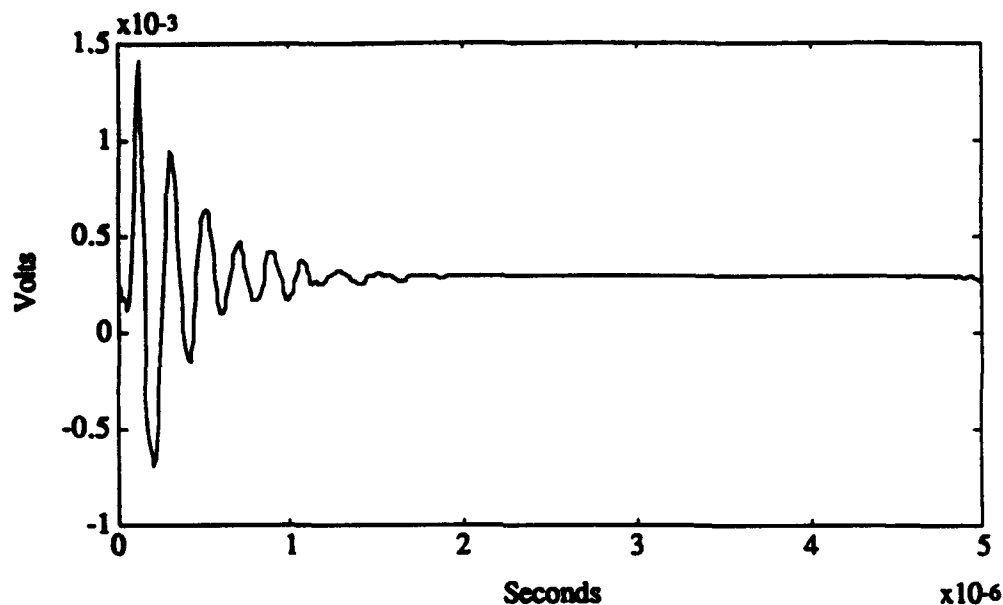
Figure 21. Predicted core voltage with 50% circumferential fault.
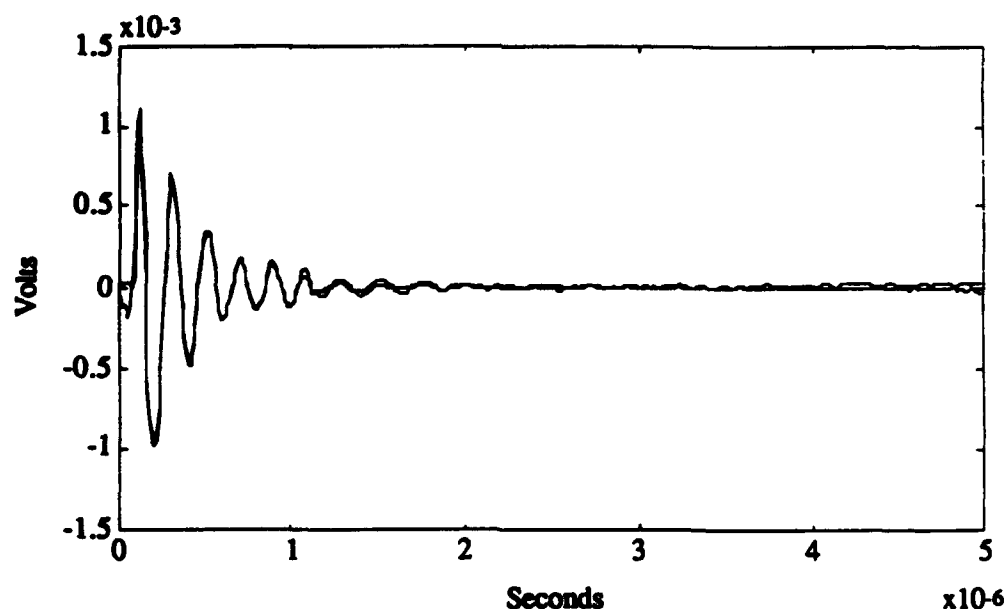
Figure 22. Overlay of predicted and measured core voltage.

26

How important is a 50% circumferential fault? A shield current of 100 A would produce 2 V with this fault (at 5 MHz), but because of the inductance, higher frequency components in a coupled shield current would produce larger voltages.

Finally, a "transfer impedance" plot from the ratio of the frequency transform of the measured core voltage to the frequency transform of the driven shield current. demonstrates the equivalence of time and frequency domain techniques (when there is adequate dynamic range and a low enough noise floor). This is shown overlaid on the CW measurement of the fault response in Figure 23.
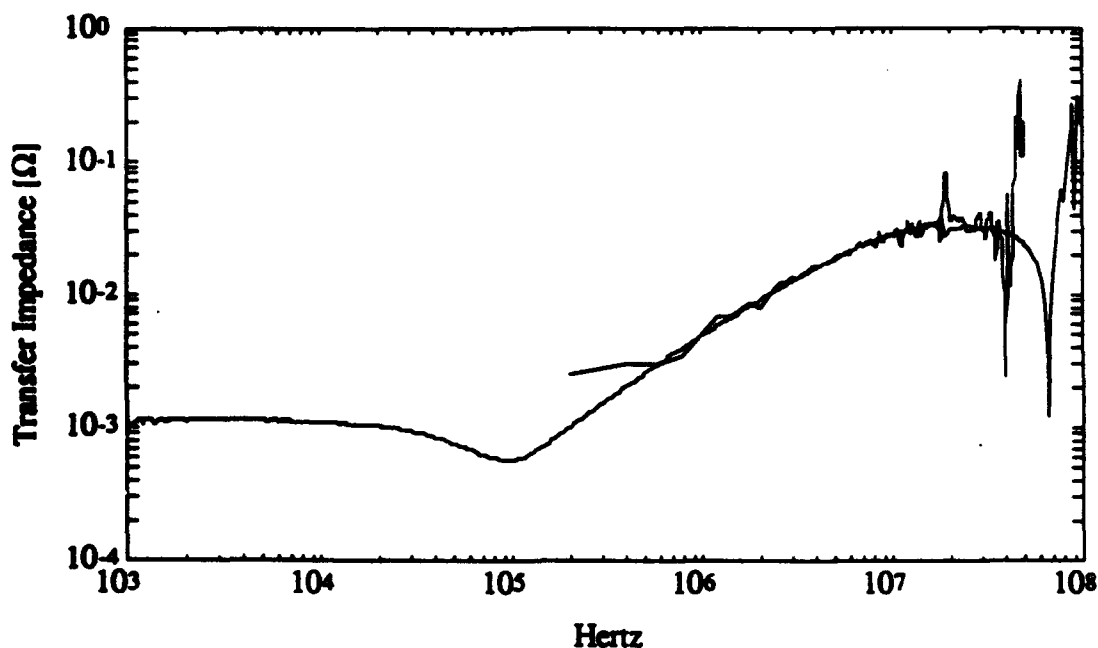
Figure 23. "Transfer impedance" acquired through pulse measurements compared to direct CW measurement.

4.2.2   High Level Pulser

To increase the drive current (and hopefully gain dynamic range) a high level pulser to drive current on the cable was set up. The basic test setup was to charge a high voltage capacitor and discharge it through a spark gap onto the cable. A 0.005-μF capacitor combined with the self inductance of the test cable created a damped sine wave of 3 MHz. In an initial test, the charge voltage on the capacitor was taken to

10-kV. This resulted in a peak shield current of about 3 A. The maximum charge voltage was 50 kV so the peak drive current for the test setup was about 15 A. Past experience has shown that for high level pulsing, energy coupled to the oscilloscope, even when external shielding is added, limits the noise floor well over 10 mV. In the baseline condition of the cable 15 A would produce less than 1 mV on the core wire, well below the noise floor of the scope. Because of these limitations no further effort was taken to pursue the high level pulse approach.

5.0 TEST CABLE CHARACTERIZATION

In a complex cable any time there are separately shielded cables such as twisted shielded pairs (TSP), coax, or triax inside a common overbraid, the effective shielding provided for the core wires of each inner cable is different. If the goal of a shielding test is to evaluate the shielding provided to the core wires, then separate measurements need to be made for each of the inner cables. If there were 20 TSPs in a cable assembly then it would require 20 measurements to correctly evaluate the shielding on each wire. However, for most cables the shielding provided by TSPs, coax and triax is only meant to reduce internal coupling between the wires. The overbraid of a cable assembly is what was designed to mitigate the effects of EMP, lightning and external EMI. The inner shields do contribute to the overall shielding of the core wires but this should be considered as a bonus and treated as extra safety margin. To properly evaluate the hardness of a cable requires that the shielding provided by the overbraid be evaluated.

To evaluate the shield of a cable an internal wire must be instrumented to measure the coupling. To evaluate just the overbraid of a cable requires an isolated conductor with shielding only provided by the overbraid. In some cables however such a wire is not available. This occurs when a cable is comprised of only TSPs, triax, or coax which have their shields terminated in the connectors. If an inner conductor on such a cable is used as a sense wire then the shielding provided by the TSP, coax, or triax is also included in the measurement. This level of shielding may not be the same for the different conductors in the cable.

The aircraft cable used as a model for the test cable was such a cable. For testing purposes a trace wire was added to the test cable. In making measurements on the test cable three different sense wire configurations were used, trace wire, inner triax shield and triax core. The trace wire measurements correspond to how the overbraid is best measured. Using the inner shield of one of the triax cables corresponds to how such a cable will probably have to be measured unless the cable is modified. Using the core wire of one of the triax cables corresponds to the core wire total shielding.

Another test variation that was also made was to terminate the switches of the inner shields of the triax cables at the test end of the cable. When the inner shields are terminated the test setup corresponds to the normal installed configuration. When the

29

inner shields are floating the test set up corresponds to a normal SCT test configuration.

Early on in the test cable evaluation process, it became apparent that averaging and shielding the voltage measurement channel were needed to improve the noise floor of the test setup. It was also observed that the joints in the multiple-piece brass fitting were dominating the braid response at the higher frequencies. Many of the measurements are obviously below the noise floor of the test setup. For certain measurements extra effort was taken to improve the noise floor by averaging 256 times and by shielding the instrumentation cables better.

5.1   TEST CABLE BASELINE RESPONSE

To characterize the complex cable each of the components was first measured separately. Figure 24 shows the response of the inner shield of the 35-in-long triax cables. The outer shield of the triax is terminated at both ends with pigtails. The length of these pigtails will affect the cable response. Figure 25 shows the response for two different length pigtails with both the inner and outer shields attached.

Evaluating the overbraid was a little more difficult. Because of the construction of the cable, the expected high frequency response of the overbraid should be basically zero. The first measurements showed definite coupling at higher frequencies in the form of a DC resistance (see Figure 26). Using a micro-ohmmeter it was quickly determined that the DC component was the resistance across the two joints which had RF gasketing. The test setup was then modified to drive current only on the overbraid. The trace wire was shielded inside the brass fitting and copper interface box so that it was only exposed in the section containing the overbraid. A piece of double thick overbraid was also placed over the RG-141 voltage instrumentation cable. The data were then averaged 256 times (Figure 27 shows the results). A very small DC value still lingers at the high frequency but that is most likely caused by coupling to the test setup which was not eliminated. The conclusion of this test is that there is no measurable coupling at higher frequencies through the triple layer outer braid. All the coupling will come from the connectors attached to this cable. When the triax cables were added to the test setup they reduced all the responses. Just by adding the
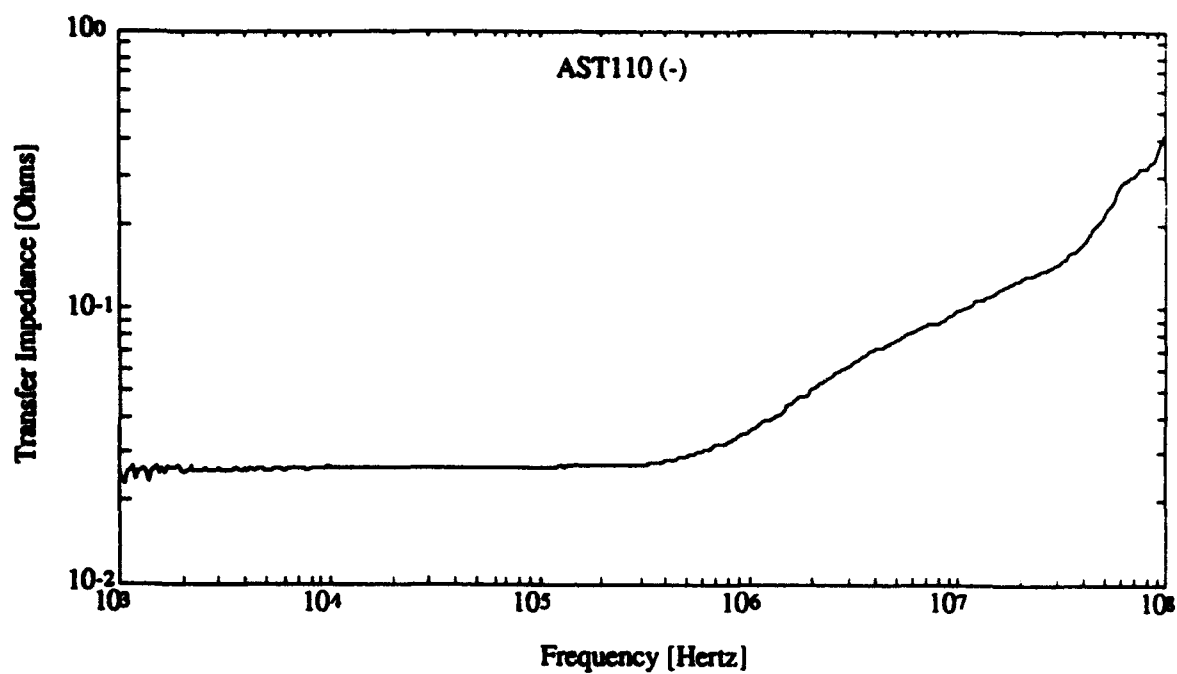
30

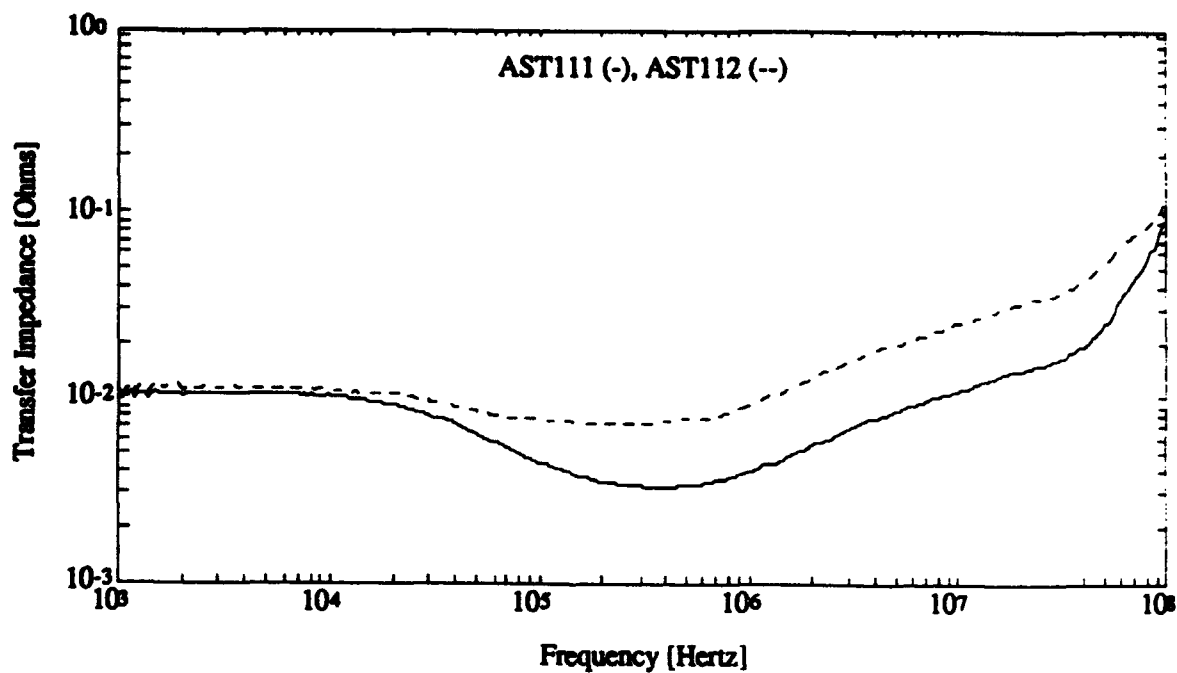Figure 24. Transfer impedance of inner shield of the Triax cable.

Figure 25. Transfer impedance of the combined inner and outer shields of the Triax cables with the outer shield terminated with different length pigtails.
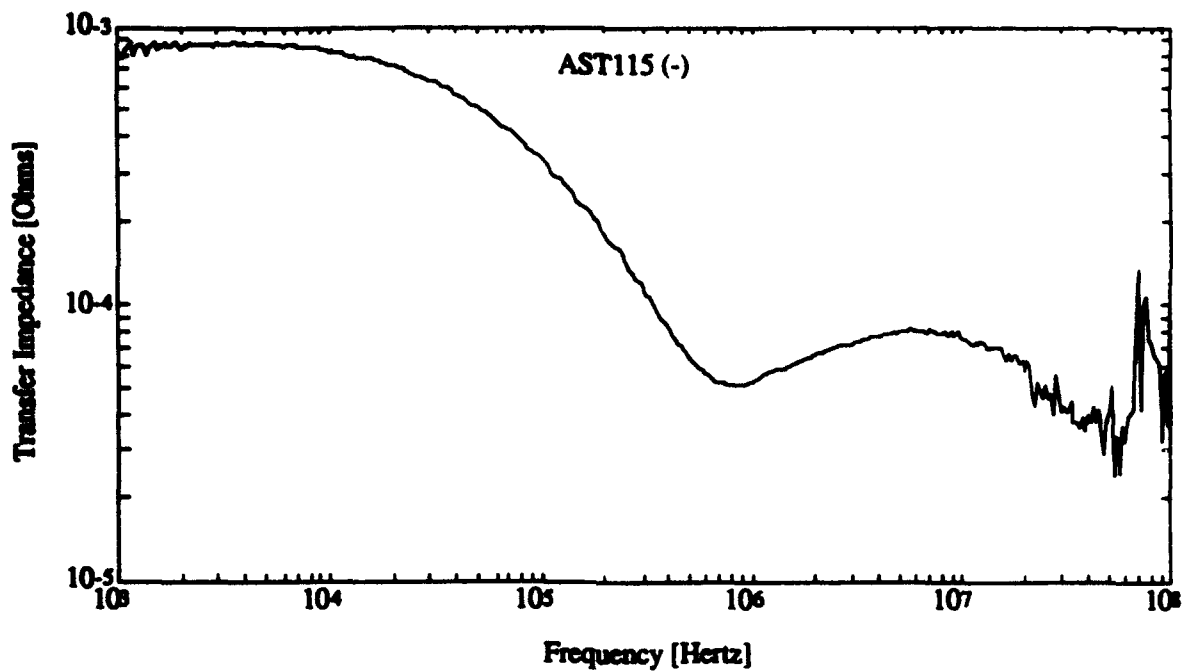
Figure 26. Baseline response of outer braid, including the brass fittings.
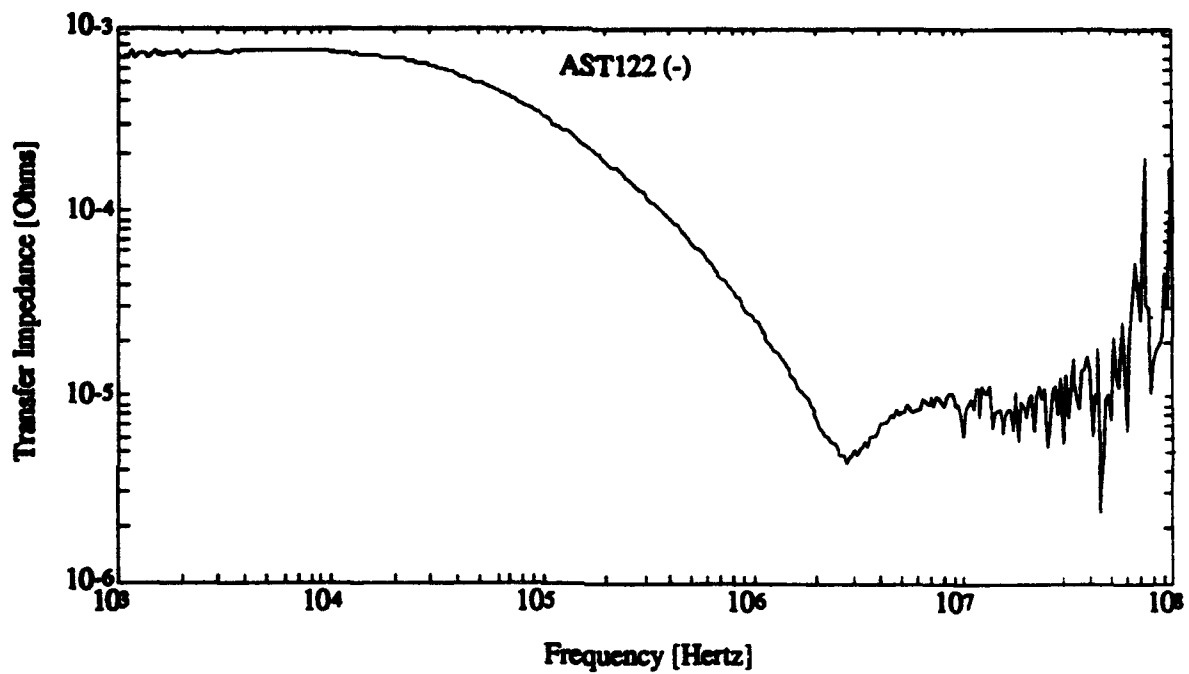
Figure 27. Baseline response of triple layer braid only.

shields in parallel with the overbraid reduces the DC response and current sharing inherently reduces coupling at higher frequencies.

The complexities of the current sharing are unique to each cable configuration; explaining them for the test cable would do little to predict them for an actual cable. The actual transfer impedance of the inner triax shielding is much more significant. Figure 28 shows the response of the complete cable mockup with nine triax cables installed. Measurements were made using as the sense wire, a trace wire, the inner shield of a triax and the core wire of a triax. These measurements were made using the power amplifier and no other effort to improve the noise floor, so the higher frequency responses should not be considered as accurate. A separate experiment was done with only a single triax installed and these data were averaged 256 times. Figure 29 shows overlays of these trace wire, inner shield and core wire responses.

Figure 28. Baseline response with all triax cables installed, using as the sense wire, trace wire (AST041), an inner triax shield (AST040) and a triax core (AST039).

33
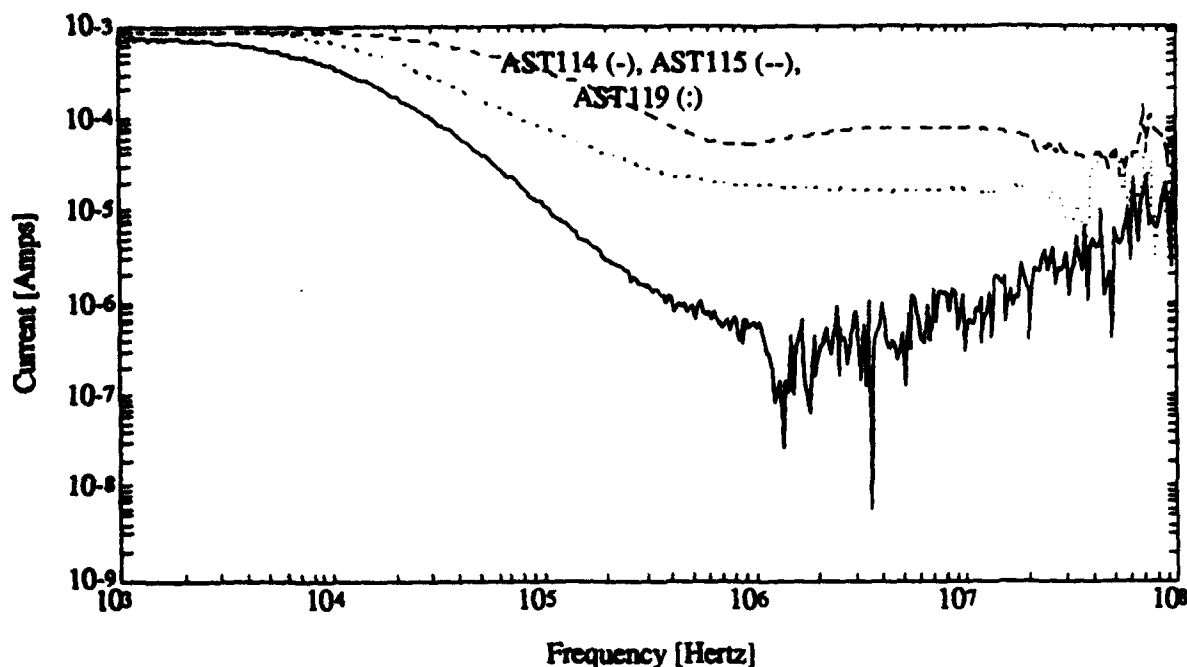
Figure 29. Baseline response with a single triax installed, using as the sense wire, trace wire (AST115), and inner triax shield (AST119) and a triax core (AST114).
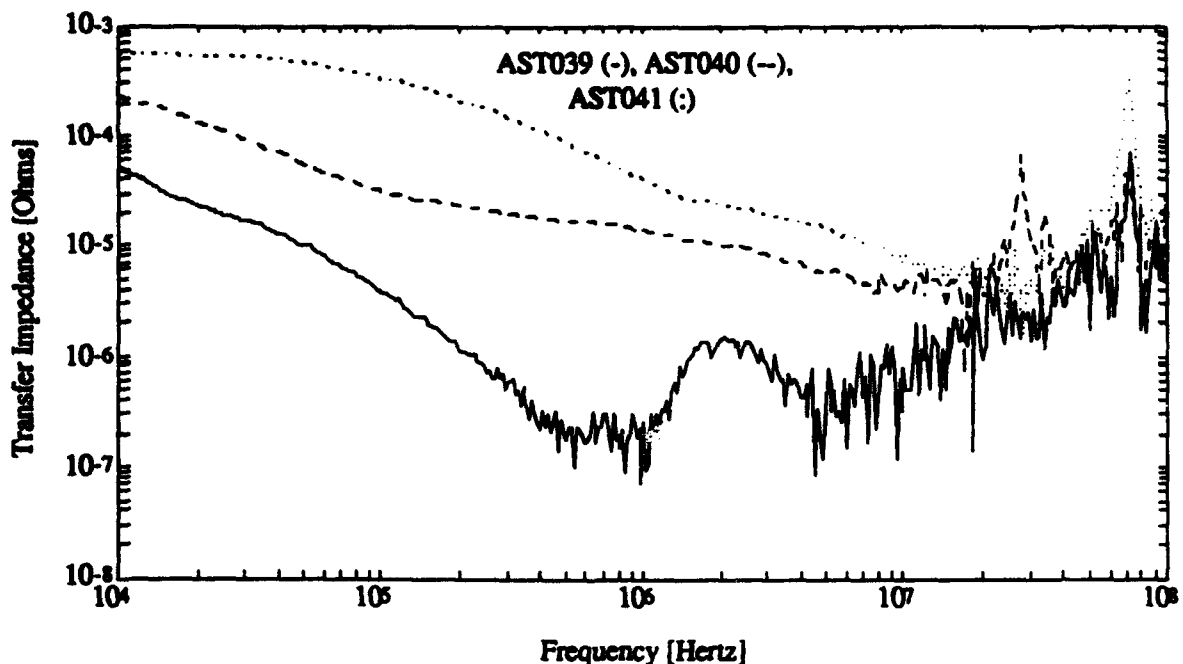
5.2   TEST CABLE FAULTED RESPONSES

Experiments were conducted to determine the effect of adding various faults to the test cable. Faults included DC faults in front of and behind the tag ring, holes through all three layers of outer braid (a slot and a 50% fault), a 100% circumferential faulting of the outermost layer of overbraid, and the disconnection of the external triax shield at the tag ring.

5.2.1   Inductive Faults

Separate measurements were taken using as the sense wire, the trace wire, an inner shield and a core wire. Overlays are made of baseline, 50% circumferential fault in all three layers of overbraid and a 1/2" slit fault in all three layers of overbraid. Figures 30 through 32 show the overlays for the three different sense wires configurations. The faults are easily seen when the trace wire or inner shield is used for the sense wire. However, when the core wire is used as the sense wire the fault responses are in the noise.

34
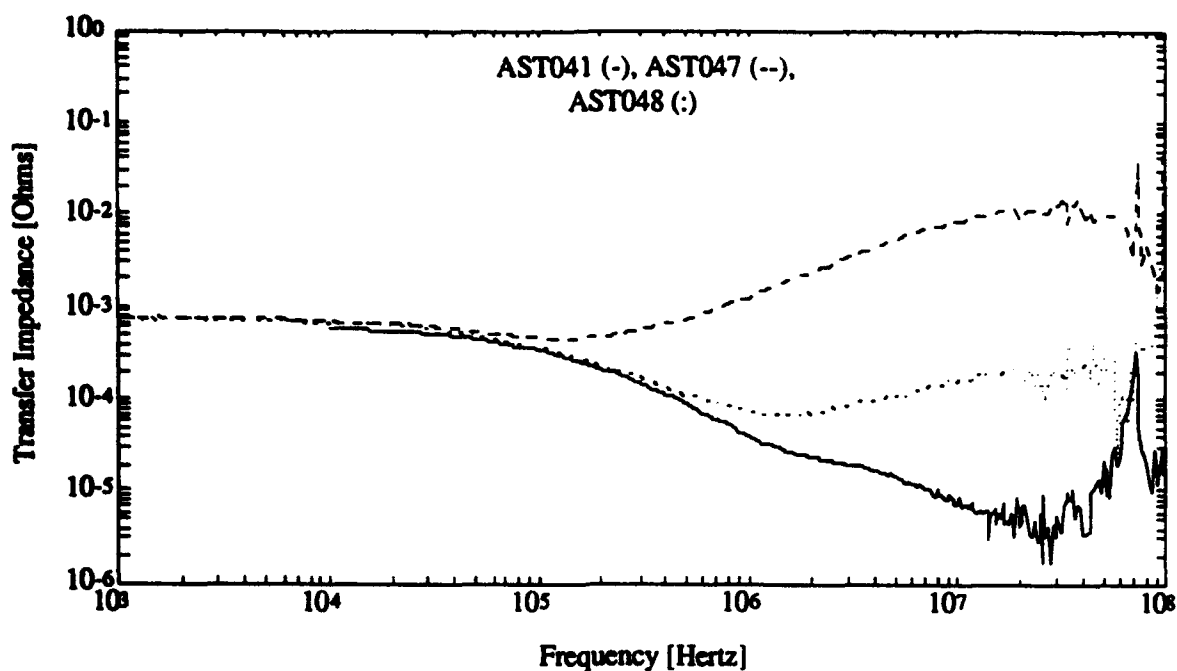
Figure 30. Using the trace wire for the sense, baseline (AST041), 1/2" fault (AST048), and 50% fault (AST047).
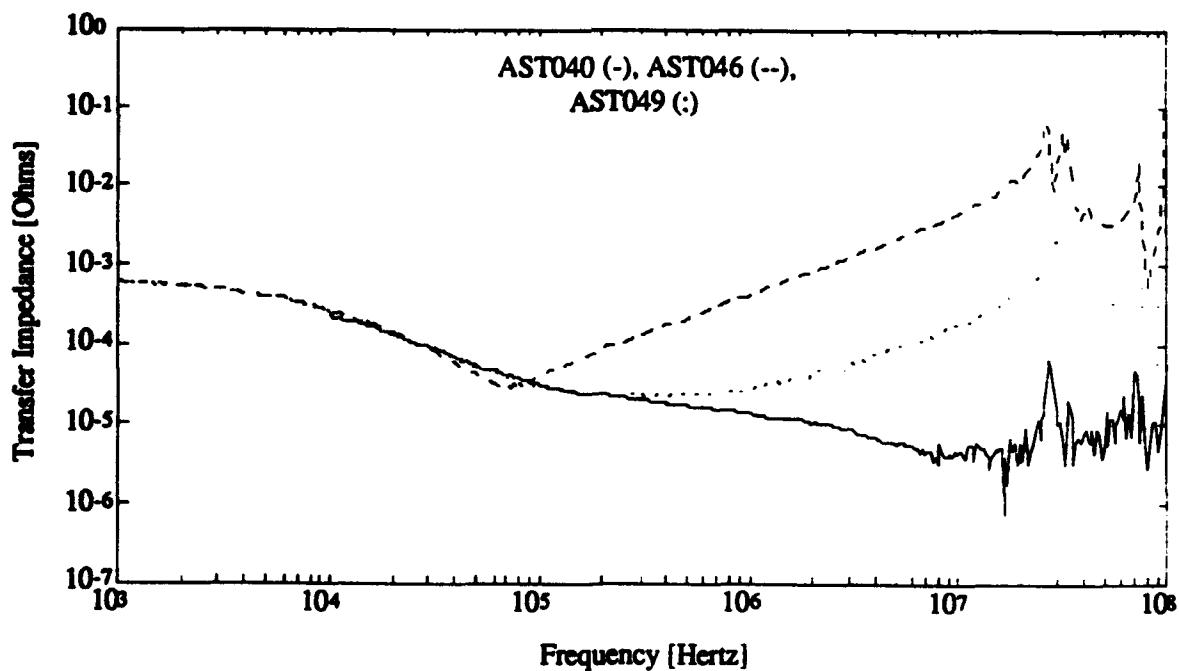
Figure 31. Using an inner shield for the sense, baseline (AST040), 1/2" fault (AST049), and 50% fault (AST046).
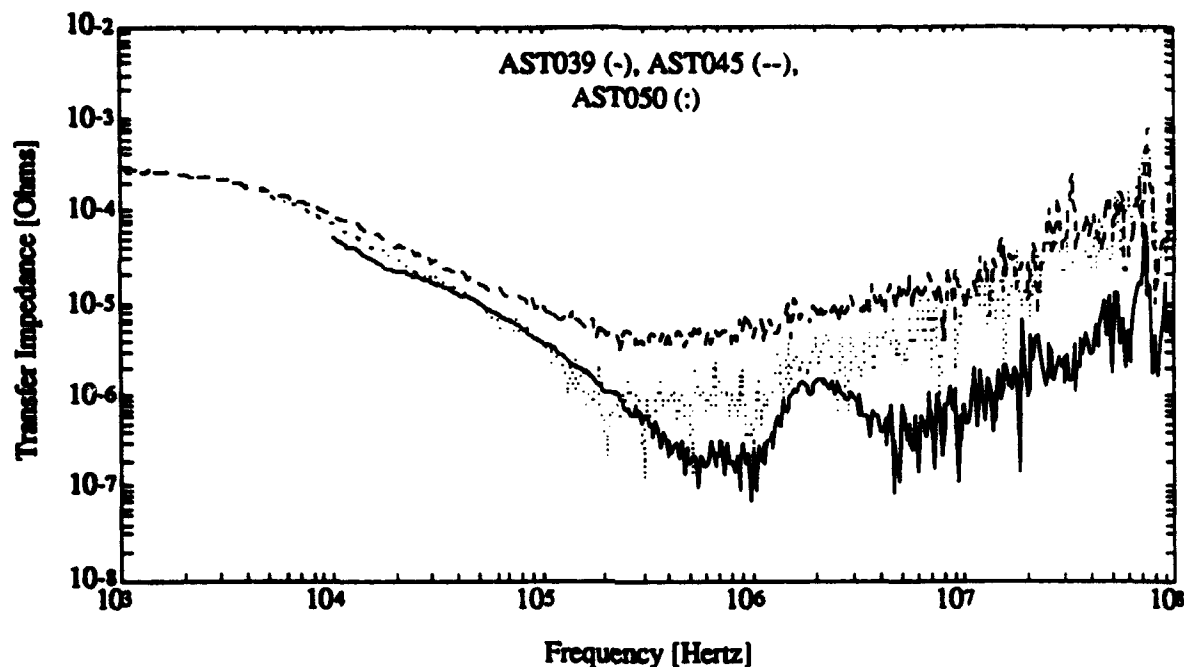
Figure 32. Using a triax core wire for the sense, baseline (AST039), 1/2" fault
(AST050), and 50% fault (AST045).

5.2.2 The DC Faults

The DC faults were included to estimate the effect of corrosion in the connector
backshell. A 100-mΩ fault was placed behind the tag ring and then in front of the tag
ring. Figure 33 shows the response measured on the core and inner shield when the
fault is placed in front of the tag ring (between the tag ring and the connector).
Figure 34 shows the faulted response when the fault was placed behind the tag ring.
When the fault is in front of the tag ring the fault is bypassed somewhat by the external
shields of the triax. When the fault is behind the tag ring this does not happen.
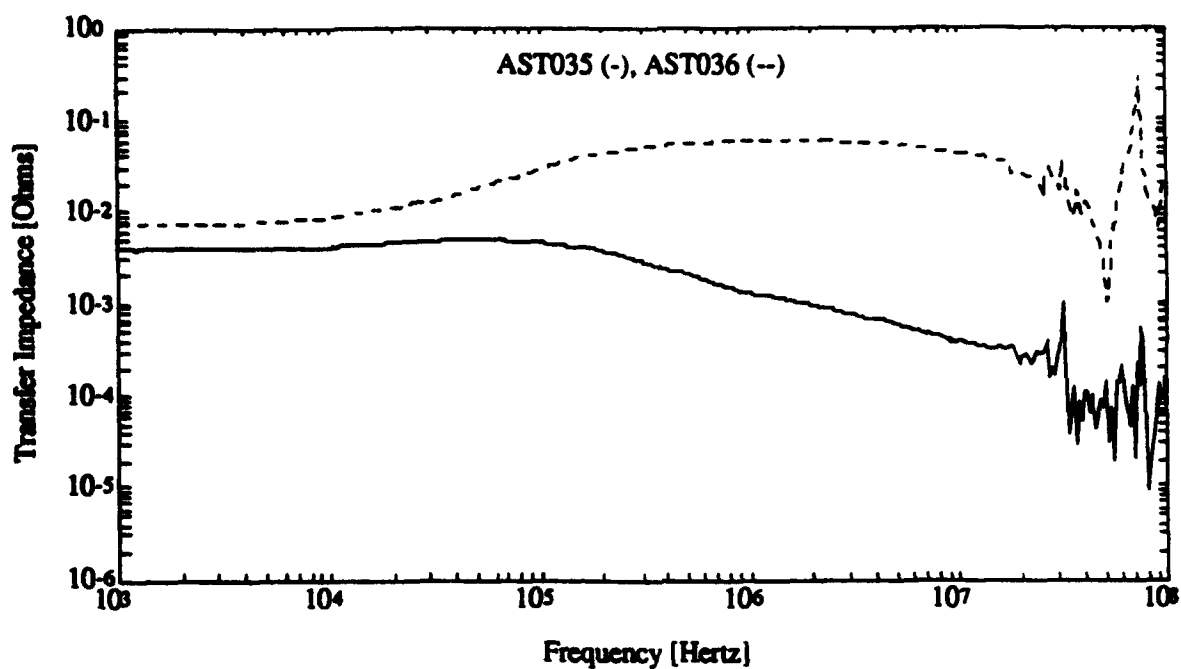
Figure 33. Response of 100-mΩ fault placed in front of the tag ring.
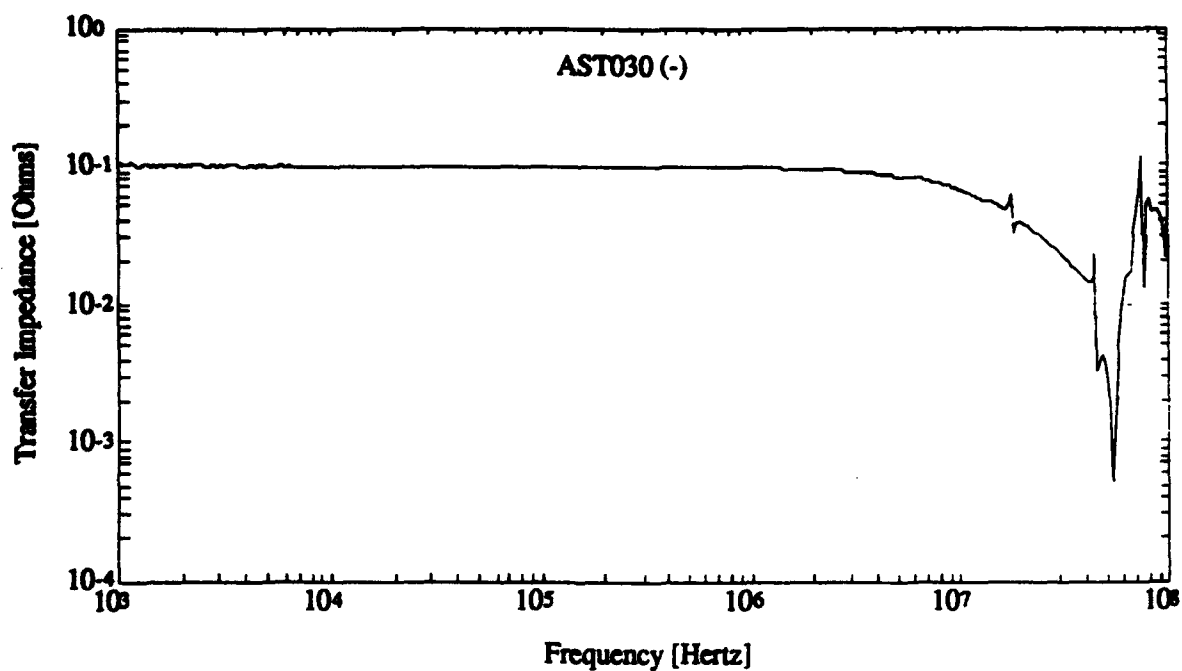
Figure 34. Response when 100-mΩ fault is placed behind the tag ring.

5.2.3 Outer Braid Fault

One type of fault that has been of concern on the aircraft has been the total separation of the outer overbraid layer from the connector. This is visually an obvious fault. To determine the electrical effects of this test cable was configured with only the three layers of outer braid and ` .ce wire. The outer layer of braid was pulled back totally from the brass connecto, .erface and the foil and inner braid left in place. Figure 35 shows the test cable response with and without the braid pulled back. These data were averaged 32 times. Since there was no significant difference between the two measurements other than a change in the DC resistance of the brass fitting, the setup was changed to remove the effect of the brass connectors and focus only on the braid response. The data were then re-taken, averaged 256 times, and compared to the same setup without the braid pulled back. Figure 36 shows this comparison. The change due to the braid fault is very slight, and detectable only in a laboratory environment.
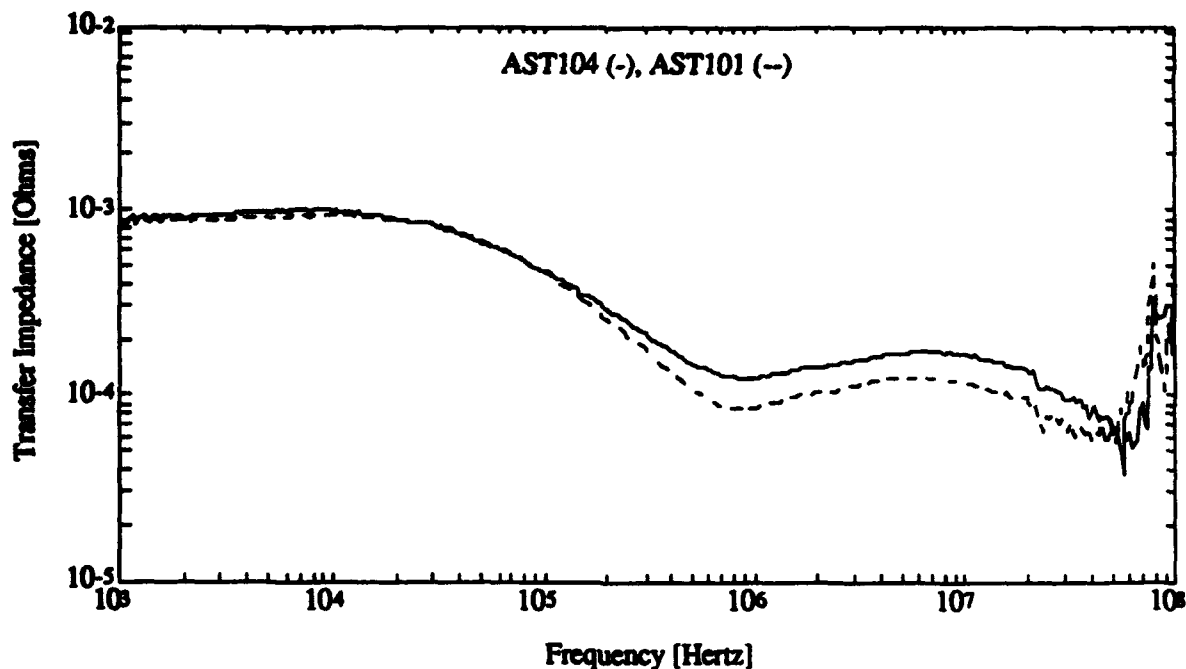
Figure 35. Response of overbraid with brass fixture, baseline (AST101) and with outer layer of overbraid pulled back (AST104).
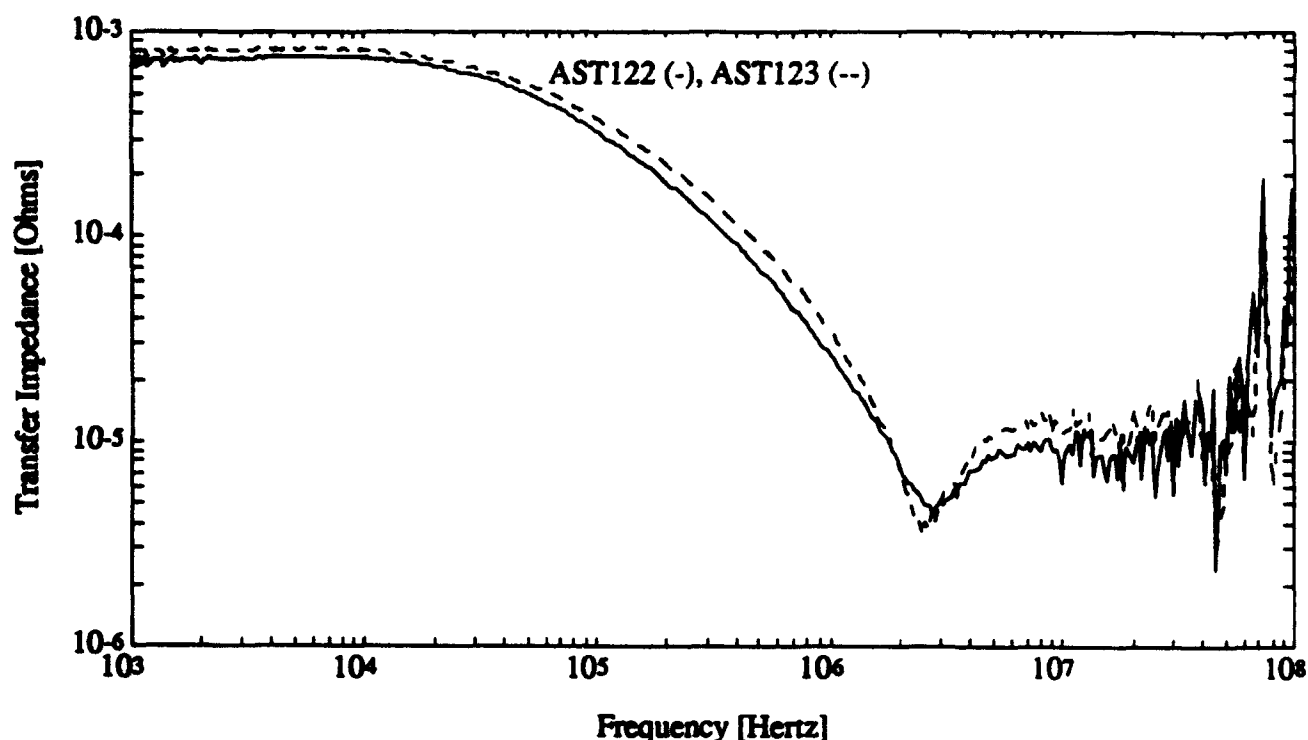
Figure 36. Response of the braid only, baseline (AST122) and with the outer layer of overbraid completely pulled back (AST123), data averaged 256 times.

When the outer layer of overbraid is pulled back, the R_{dc} value increases slightly (and the skin depth roll-off occurs at a slightly higher frequency). This happens because, for the distance between the connector and the last electrical contact point between the outer layer and the copper foil, the effective cross sectional area of conductor is reduced (recall the formula for calculating the resistance of a wire, which is shown below).

$$R = \frac{l}{g A}, \text{ where}$$

l = length,
g = conductivity,
A = cross sectional area.

The SCT was able to detect a small difference when the braid was pulled back. The measurement was 0.71 mΩ with the braid intact, and 0.78 mΩ with the braid pulled

back. This 0.07-mΩ difference can also be detected by a micro-ohmmeter, but it is below the present threshold of the TIM. It is critical to note, however, that this difference is more than an order of magnitude below the typical contact impedance of a pristine connector (about 1 mΩ). This type of difference was detected repeatably in the laboratory, but it is not reasonable to expect this level of stability in an in-situ test setup. Both the test setup and the actual connector joint contact impedances will vary much more than 0.07 mΩ between surveillance measurements.

5.3   EFFECTS OF MATTING CONNECTORS

In real life any installed cable has connectors attached to it at both ends. Like the test cable, energy couples through them to the core wire. The response of a cable assembly is determined by the combined response of the cable and both connectors. The transfer impedances of these component parts add directly. Adding a brand new connector pair to the test cable changes the response dramatically. Figure 37 shows an overlay response of the cable braid only, the cable braid with the brass fixtures, and the cable braid with brass fixture and connector pair. The addition of the brass fixtures and connector pair have added DC components to the cable assembly response over the entire frequency range. At the lower frequencies the effect of these components is small, however, at the higher frequencies they totally dominate the response of the test cable. The connector which was added was the same type found on the aircraft cables the test cable was modeled after. It made a very tight connection and actually had low contact resistance (<1 mΩ) compared to typical fielded connector pairs.

Since connectors are part of any cable assembly the real question is how do faults appear when combined with the effects of a connector pair. Two sets of experiments were conducted combining the effects of faults and the connector pair. Since the contact resistance of the connector pair can vary greatly and these experiments were done at separate times, the observed DC responses will vary. Since this connector pair had a very low contact resistance (<1 mΩ), the contamination effects will not be as great as would be seen with a fielded cable assembly.
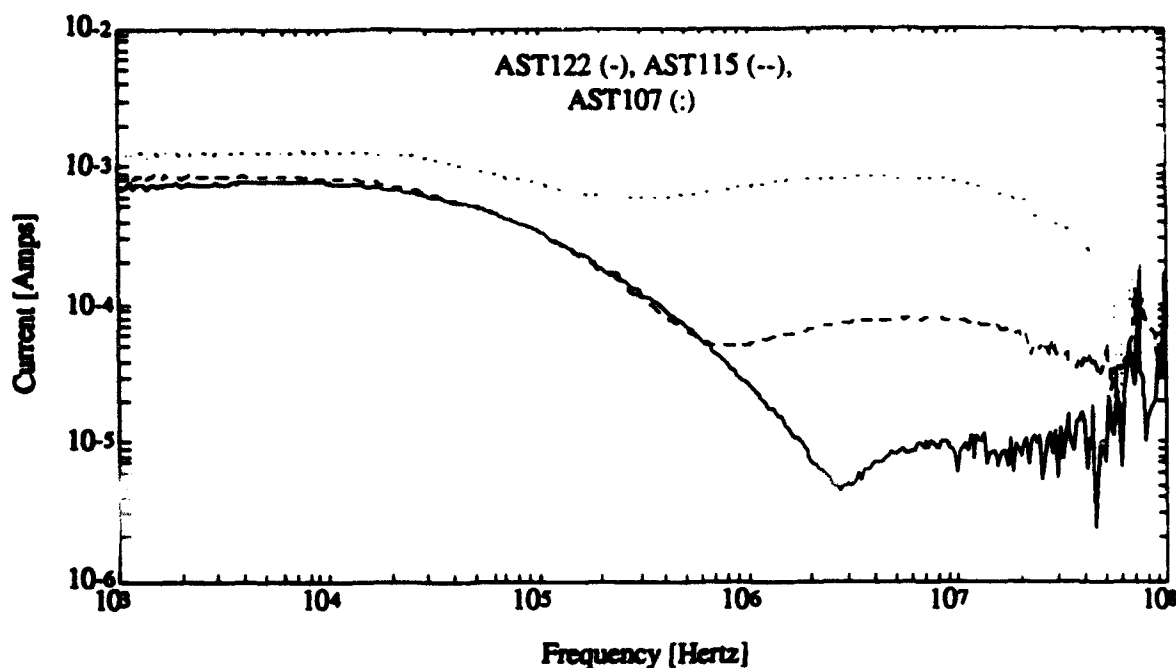
Figure 37. Overlay of responses for braid only (AST122), braid plus brass fixture (AST115) and for braid plus brass fixture plus connector pair (AST107).

The first experiment had the test cable configured with the triax cables and a trace wire installed inside the overbraid. Measurements were made using the three different sense wires (trace, inner triax shield, and triax core). Figure 38 shows measurements taken with the trace wire in the baseline, connector baseline and when the connector is combined with the 1/2-in fault and 50% faults. Figure 39 shows the same measurements when using a triax inner shield for the sense wire and Figure 40 when using a triax core wire as the sense wire. The data show that the small 1/2-in fault is hidden by the response of the connector. The large 50% fault is visible, however.
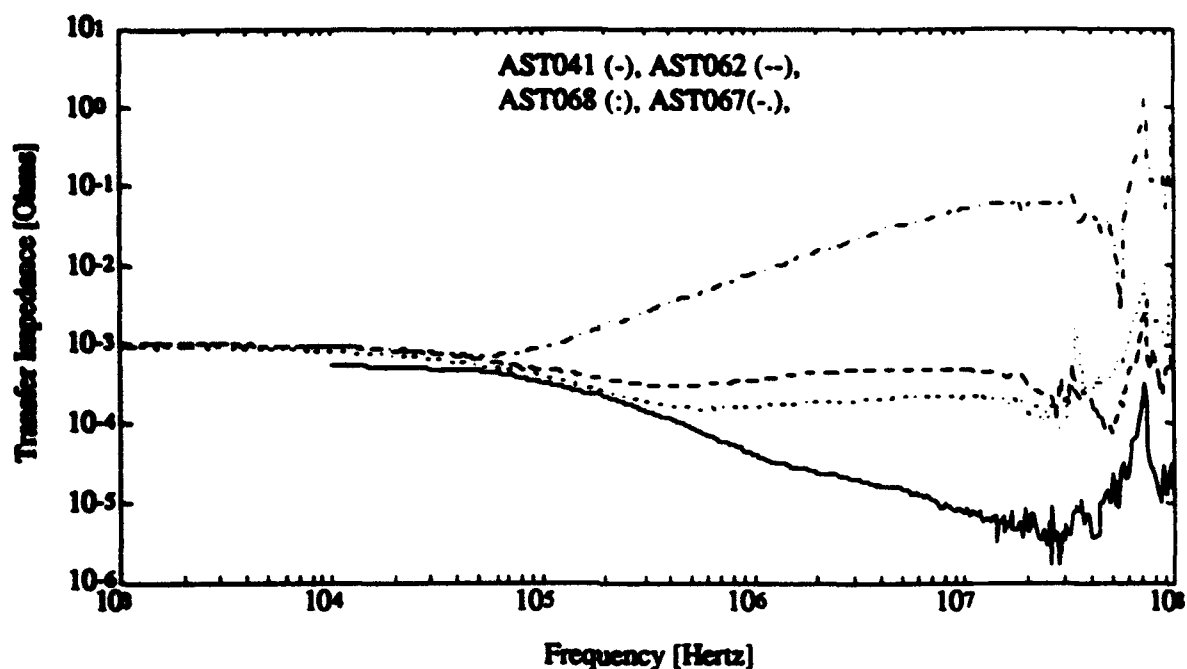
Figure 38. Using trace wire, braid only (AST041), with connector pair (AST062), with connector and 1/2-in fault (AST068), and with connector and 50% fault (AST067).
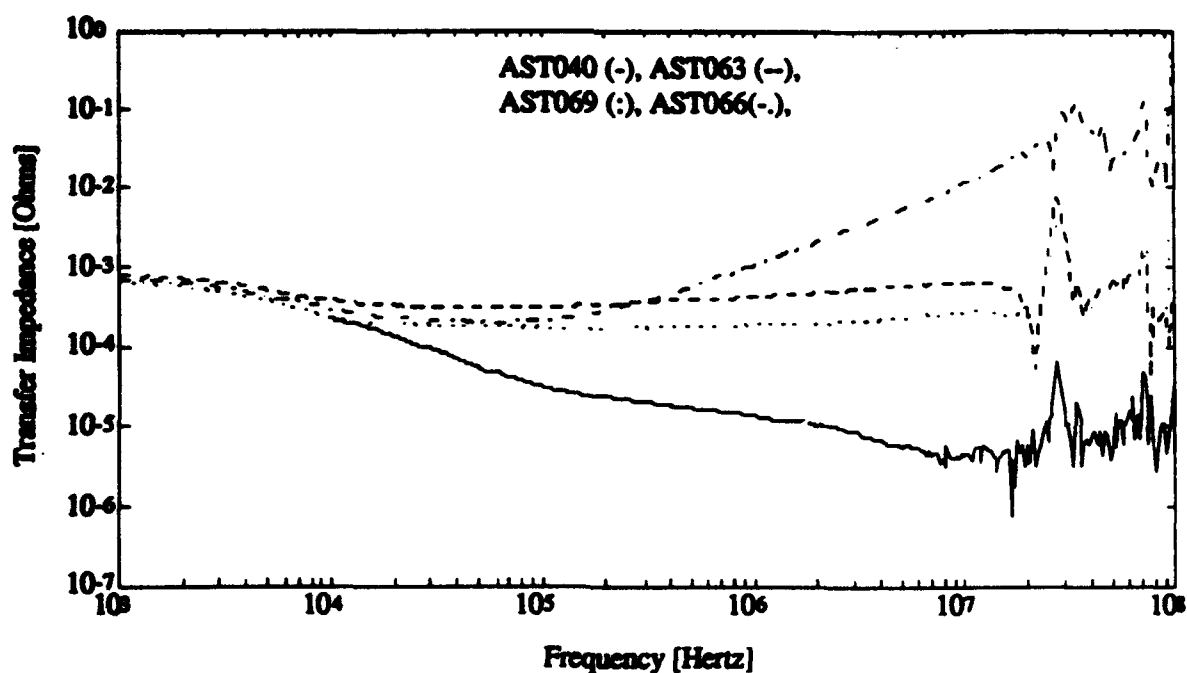
Figure 39. Using inner shield, braid only (AST040), with connector pair (AST063), with connector and 1/2-in fault (AST069), and with connector and 50% fault (AST066).
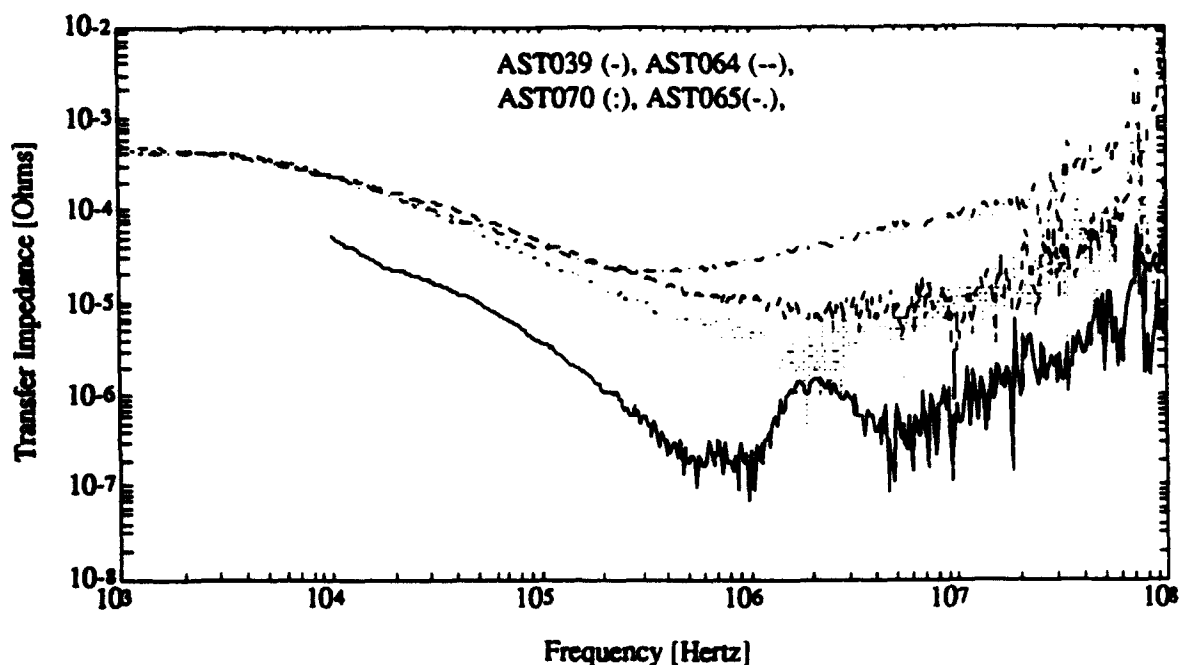
Figure 40. Using triax core, braid only (AST039), with connector pair (AST064), with connector and 1/2-in fault (AST070), and with connector and 50% fault (AST065).

The second experiment looked at the combined effect of the outer overbraid fault and the connector pair. This experiment used just the three layer cable overbraid and a trace wire. Figure 41 shows an overlay of the braid only response with the outer layer pulled completely back versus the unfaulted braid response combined with the brass fixture and connector pair. As expected the effect of the connector pair is orders of magnitude above the shield fault. There was no way to electrically detect this type of fault with the laboratory setup when compared with an overbraid only baseline. There is absolutely no way this fault will be detected in the field when combined with the response of connectors. Visual inspection is the only realistic way this fault will ever be detected.

Figure 41. Cable and connector response (AST107) and braid only response with outer braid pulled back (AST123).

5.4   SENSE WIRE ANALYSIS

In the test setup there were three different sense wire options, each one is shielded by a different number of shield layers. The co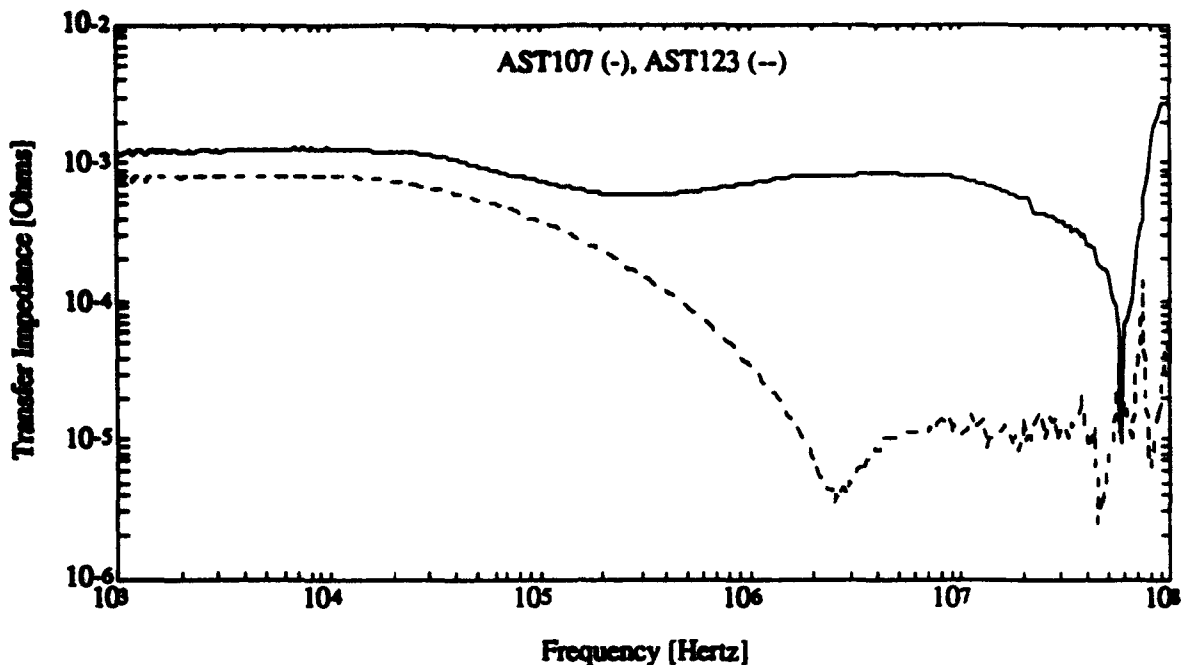re wires of the triax are shielded by the triple overbraid and both layers of the triax shields. The inner shields of the triax are shielded by the triple overbraid and the outer shield of the triax. The trace wire is only shielded by the triple overbraid. Obviously the trace wire would be most sensitive to faults in the overbraid. However, in some cables there are no inner conductors which behave as a trace wire. This includes some aircraft cables.

Using the inner triax shield for the sense wire connection may be the only option available without modifying the cable. The sensitivity of the inner triax shield to faults in the overbraid is greatly affected by the length of the pigtails used to terminate the outer shield of the triax. The longer this pigtail the greater the sensitivity. It is also affected by how far back the outer triax shield is separated from the inner shield.

These pigtails on the aircraft cable were about 1.5-in long at both ends. In the test setup the pigtails at the interface end were about this same length. The pigtails at the termination end were significantly longer. The outer triax shield in the test setup is also separated farther back than on the real cable. The net result is that the measurement sensitivity using the inner triax shield in the test setup is probably much greater than would be the case on an actual cable. This difference could be more than an order of magnitude.

Since each triax inner shield is shielded by a different outer shield, the coupling to each inner cable can be different. If an inner shield is used as the sense wire, measurements would need to be made using all the inner shields to completely characterize the cable.

This type of cable could be modified in two ways to add a trace wire. First, if there is an unused pin in each connector, a wire can be added at both ends which terminates at the inside of the overbraid just behind the connectors. This would enable testing of the connector and connector braid interface with much better sensitivity.

The second approach would be to select a present triax, if one exists, which does not have a stringent pin specification, and disconnect the pigtail termination of the outer triax shield at both ends of the cable. The inner shield of this triax will behave as a trace wire.

6.0 CONCLUSIONS AND RECOMMENDATIONS

This report shows that any shield fault, with respect to a "good" baseline, causes more coupling at high frequencies than at DC. **WITHOUT EXCEPTION, given a shield fault, there is always more of a change in shield performance between 100 kHz and 10 MHz than there is at 1 kHz.** Therefore, it is better to make a high frequency transfer impedance assessment than it is to rely solely on a milliohm meter reading and visual inspection.

Whether it is "Shielding Effectiveness" or "Total Transfer Impedance," a sure way to evaluate the **high frequency** performance of a shielded cable harness is to couple energy on the outside and measure the response on the inside. Frequency-domain testing is arguably the best approach. It provides a much better signal to noise ratio and is easier to implement than time-domain pulse testing.

As shown in this report, several modifications to the standard CW SCT test techniques would expand its useful measurement range for detecting high frequency shield faults in complex shield topologies (i.e., aircraft cables). These modifications include signal averaging, drive current and input voltage amplification, and instrumentation cabling. These improvements also apply to the field tester TIM and are achievable with additional funding.

However, until the TIM and/or SCT are improved, continued testing with the SCT and/or TIM (TIM also includes a milliohm meter mode), augmented with visual inspection, is all that is required to maintain the cable shield hardness. This approach will detect severe **high frequency** degradations that are certifiably bad and lead to tracking less severe problems that can worsen over a system lifetime.

BIBLIOGRAPHY

Hendrickson, J. T., " Shielded Cable Tester Users' Operating Manual," TRW, Albuquerque, NM, April 1988.

Coonrod, K. H. and Hendrickson, J. T., "Operation and Maintenance Instructions Transfer Impedance Meter," TRW, Albuquerque, NM, October 1992.

Hoeft, L. O., "Surface Transfer Impedance: The Intrinsic Electromagnetic Property for Specifying Cable Shields and Connectors," The BDM Corporation, Albuquerque, NM, April 1985.

Keyser R. C., Whiddon W. B., and Collette D. F., "AERO 90 EMP Hardening Elements Handbook," prepared for the Defense Nuclear Agency, Alexandria, VA 2310-3398, Doc # DNA-H-90-64, May 1991.

Madle, P. J., "Test Procedures to Measure the Transfer Impedance of Shielded Connectors, Backshells, Tubular Cable Shields, and Assemblies," prepared for the Society of Automotive Engineers Committee Meetings, AE2 and AE4, and the IEEE Symposium on Electromagnetic Compatibility, Albuquerque, NM, October 1979.

Vance, E. F., Coupling to Shielded Cables, John Wiley and Sons, Inc., New York, NY, 1978.

Appendix A

Shielding Evaluation of a Solid Copper Tube

Subject	Date	From
SLFCS Cable Transfer Impedance Measurements	11 January 1991 H903.91.KHC-01	K. H. Coonrod

To	cc	Location/Phone
Karl Auerbach	J. T. Hendrickson P. J. Miller S. L. Davis C. C. Herrmann	ANM2 (505) 768-1152

This IOC presents the results of the SCT evaluation we performed an a sample SLFCS cable. The results include baseline and faulted responses for the cable. A brief description of the test setup is also given.

The cable sample we tested was approximately one foot long. All measurements are of this one foot sample. Only the solid copper outer shield of the cable was evaluated. The cross-sectional view of the cable is shown below in Figure 1.
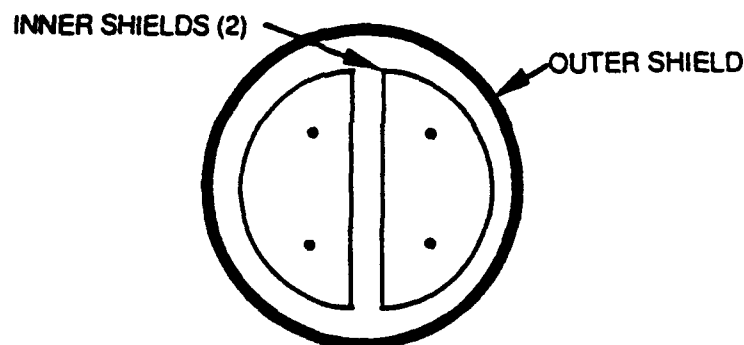

Figure 1. Cross section diagram of the SLFCS cable.

Because of the geometry of the cable, (1/16" thick solid copper shield and 1' length) any baseline transfer impedance measurement would obviously be quite small. The baseline measurement is shown as the solid line in Plot 1 (enclosed), along with the theoretical dashed line based on the following equations from E. F. Vance's "Coupling to Shielded Cables."

$$Z_T = \frac{1}{2\pi a \sigma T} \frac{(1+j)T/\delta}{\sinh((1+j)T/\delta)} \text{, and}$$

$$\delta = 1/\sqrt{\pi f \mu_0 \sigma}$$

where: a = radius
σ = conductivity
T = thickness
f = frequency
μ_0 = permeability of free space

Plot 1 shows that the theoretical response past 100 kHz "rolls off" to extremely small signal levels. The theoretical response is well below the $100\mu\Omega$ noise floor of typical SCT measurements. The baseline measurement, then, required modifications to the normal SCT setup along with a great deal of care. Figure 2 shows the modified setup, which provided a noise floor no greater than $1\mu\Omega$ at frequencies above 10 kHz, as shown in Plot 2.
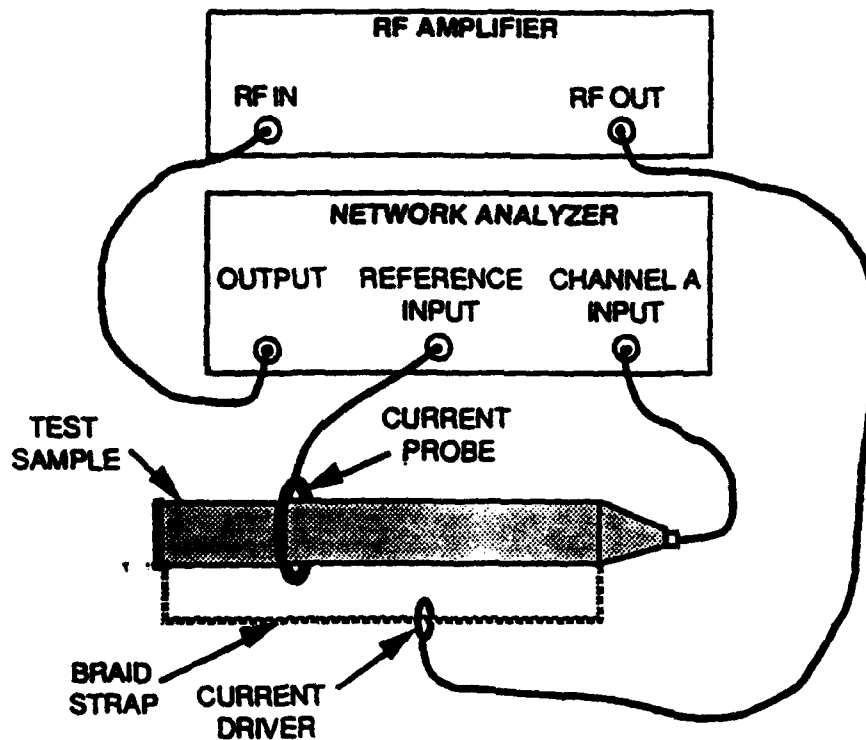
Figure 2. Basic test setup.

We used one of the inner shields as the sense wire, shorting it at one end to the inside of the outer shield. This end was then capped with a copper plate soldered in place.
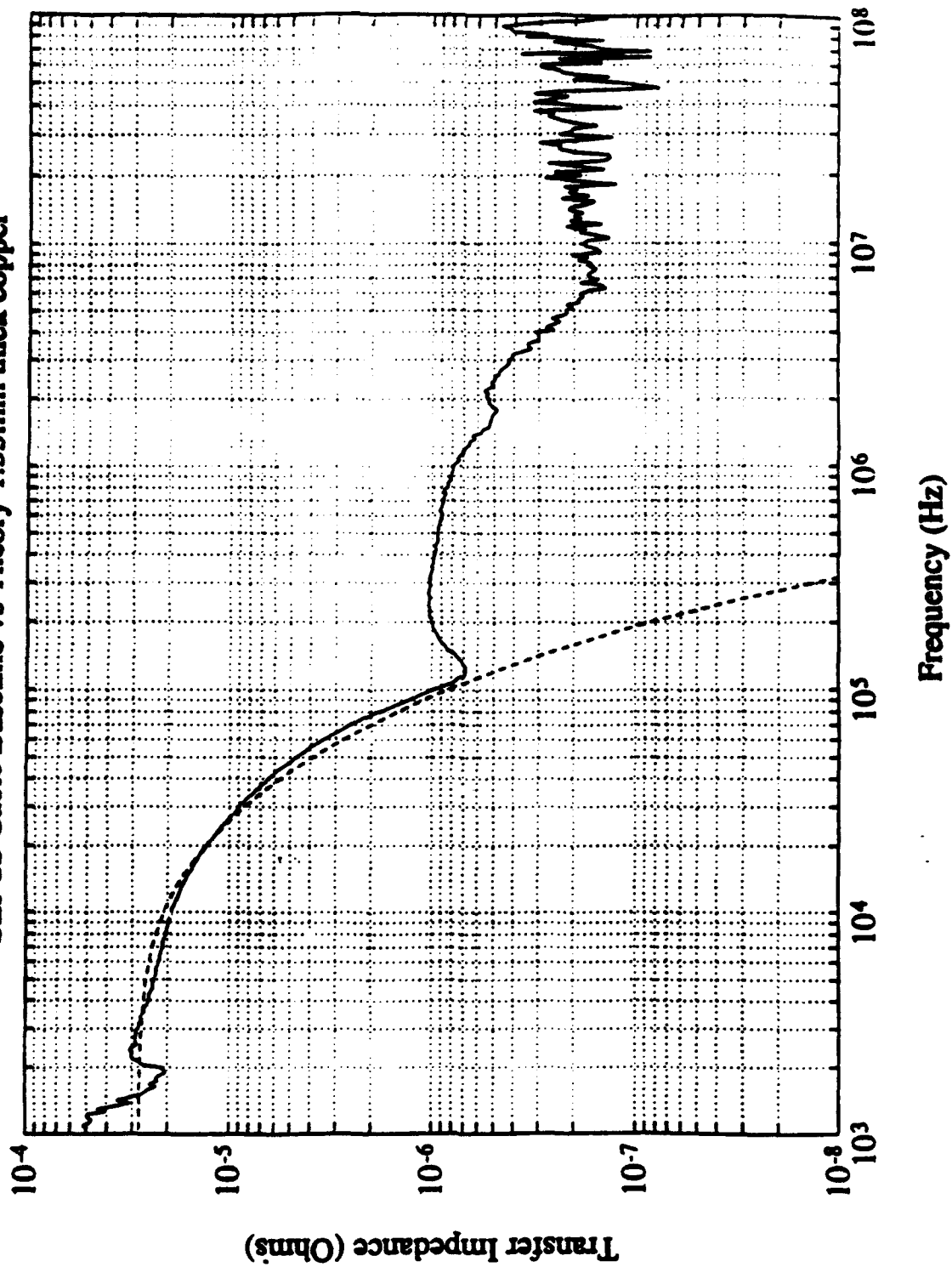
The other end of the "sense wire" was attached to an N-feedthrough connector soldered to a copper cone soldered to the outer shield. The reference current was acquired with a current probe placed directly around the sample. The drive circuit required modification in order to produce responses above the network analyzer noise floor. The output of the network analyzer was boosted with a wideband power amplifier which produced coupled currents 22 times greater than normally used with the SCT. This amplifier had poor response below 4 kHz, so data below this frequency is unreliable.

The DC response of the baseline measurement (shown again in Plot 3) was ≈ 28μΩ, which agrees well with both theory (≈ 28μΩ) and the value measured with a milliohm meter (.03mΩ). The skin depth effect also agrees well with theory. The baseline measurement diverges from theory above 100 kHz, where coupling to the instrumentation cables determines the response, then at about 5 Mhz the lowered network analyzer noise floor dominates. We modeled the instrumentation coupling as a second current loop that flowed over the copper cone and sense cable at a level about 50 dB less than the current in the intentional drive loop. The transfer impedance of the copper cone causes the small instrumentation current to couple onto the sense wire. Plot 4 shows that this explanation agrees with the baseline measurement. These coupling effects are extremely small, ranging from .1μΩ to 1μΩ, and will be shown to be insignificant when compared to coupling from shield degradations.

Several faults were made to the shield of the cable and their effects measured. The faults included a single hole of 1/8" which we incrementally enlarged to 3/16" and 1/4" diameters. Afterwards, we cut a 1/16" x 1" slit and subsequently lengthened it to 2 3/4", along the circumference of the shield over the 1/4" hole. In all cases the faults were placed directly below the current return path, thus giving a worse case response. Plot 5 presents an overlay of the baseline response and the 1/8" hole faulted response. Plot 6 presents the baseline response again along with overlays of the three different size holes. Plot 7 presents the baseline response with overlays of the two slit lengths.
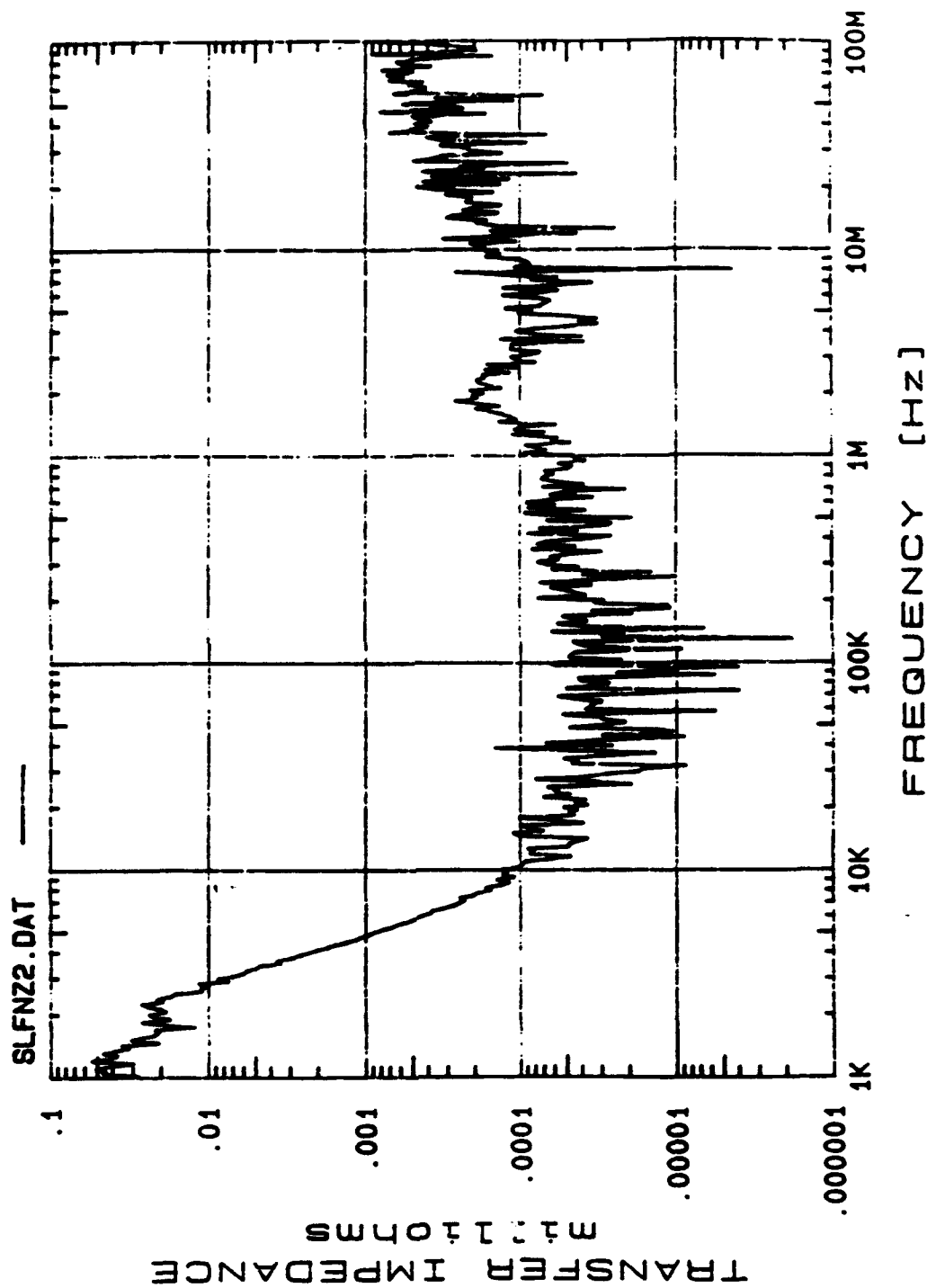
Even with the limits of the measurement technique it is easy to see that a single 1/8" hole in the shield will dominate the high frequency response. Both theory and our measurements show that coupling through an unfaulted cable at EMP frequencies is very small. However, it must be remembered that any type of connections made to this cable will not be as good as the cable itself, and these connections will undoubtedly determine the overall response of the SLFCS cable.
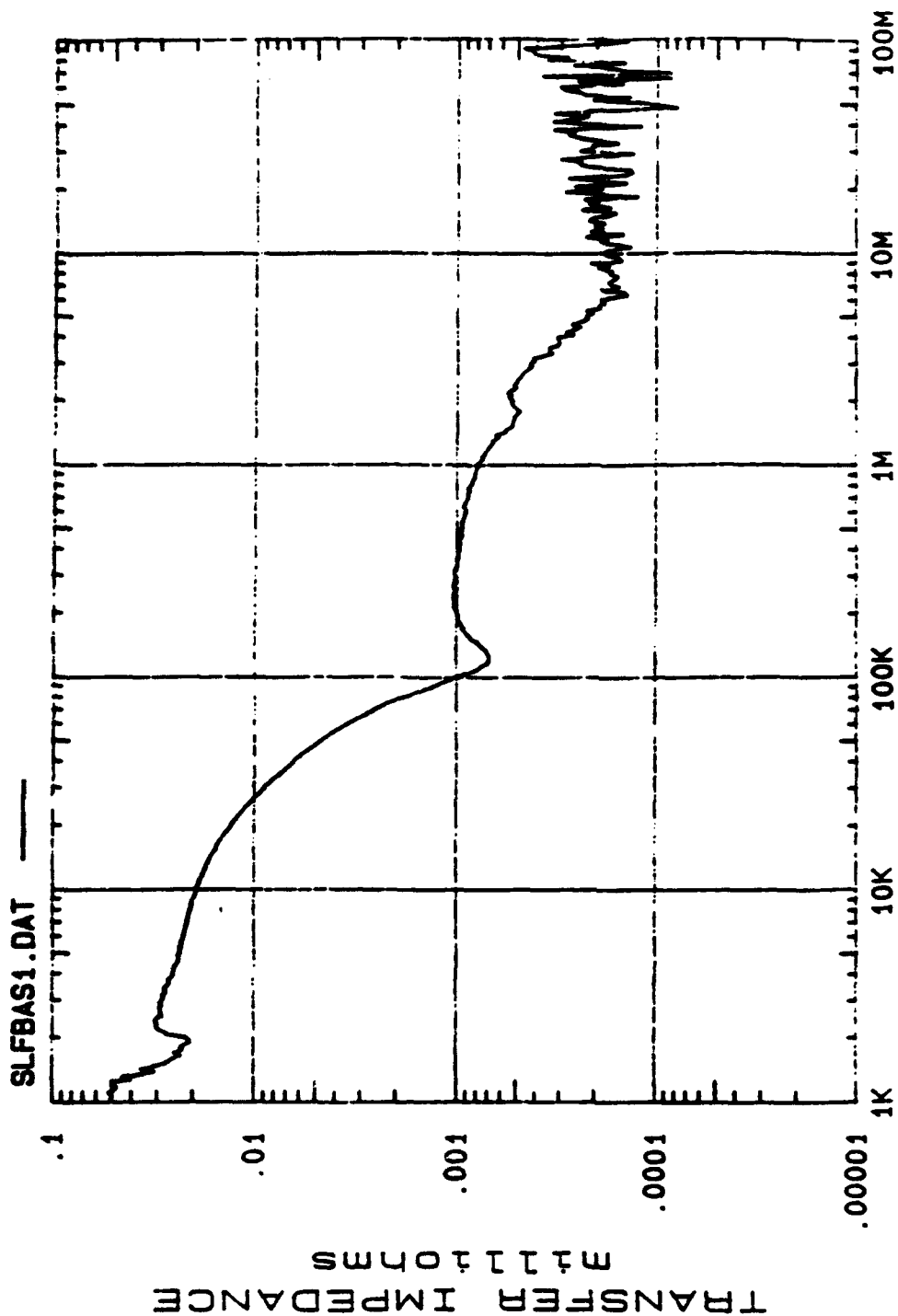
SLFCS Cable Baseline vs Theory 1.35mm thick copper

Frequency (Hz)

Transfer Impedance (Ohms)

Plot 1.

Noise measurement of the test setup.

SLFN22.DAT ———

FREQUENCY [Hz]

Plot 2.

TRANSFER IMPEDANCE m:;1:1ohms

53

Baseline response of the SLFCS cable sample.

SLFBAS1.DAT ⎯⎯⎯

Plot 1.

FREQUENCY [Hz]

TRANSFER IMPEDANCE milliohms

SLFCS Cable Baseline vs Theory t=z(.85)-z(.08)/320

Transfer Impedance (Ohms)
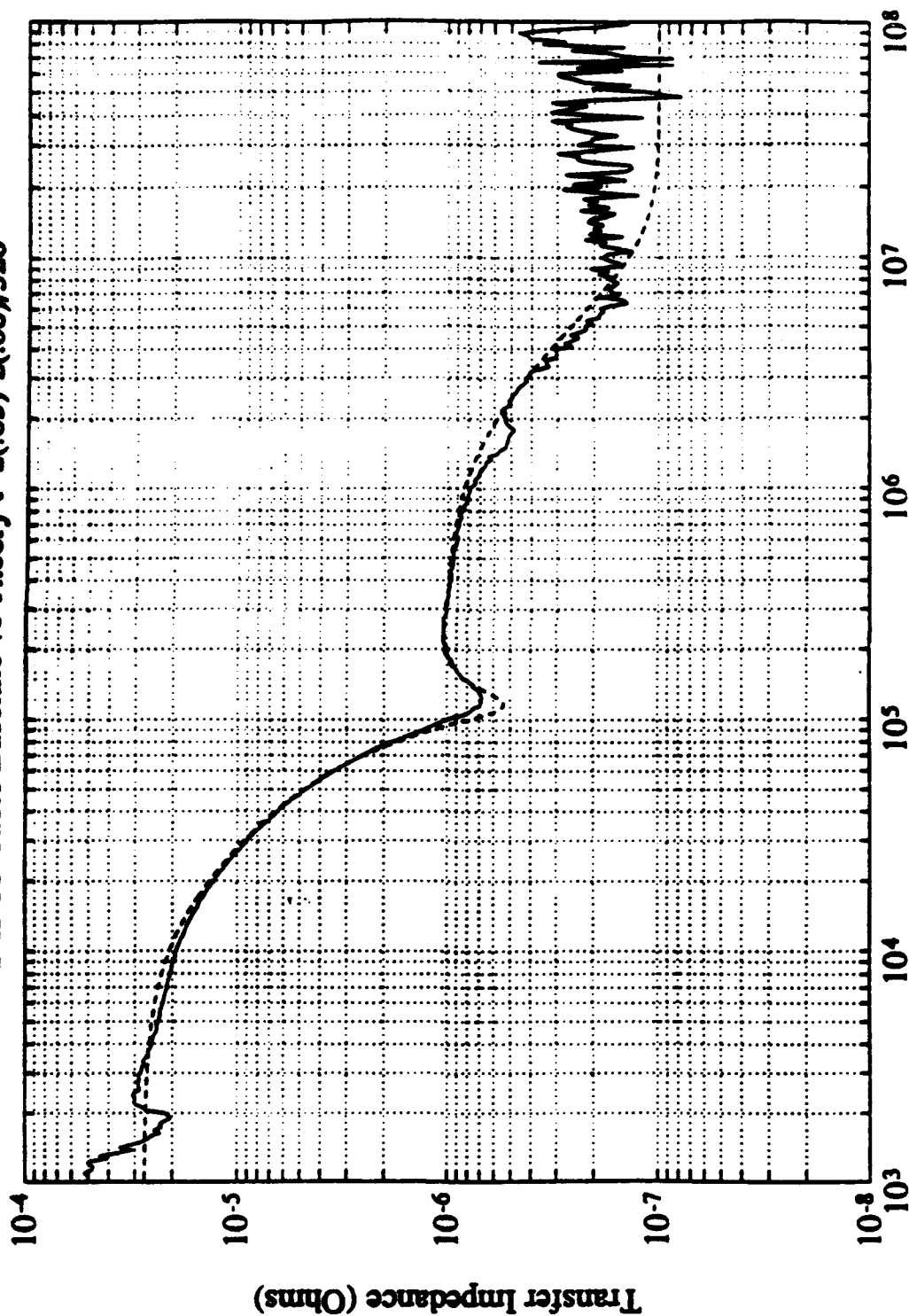
Frequency (Hz)

Plot 4.

55

Overlay of the baseline response and the response with a
single 1/8 inch hole.

SLFBAS1.DAT ——— SLF1_8.DAT ———

FREQUENCY [Hz]

Plot 5.

TRANSFER IMPEDANCE milliohms
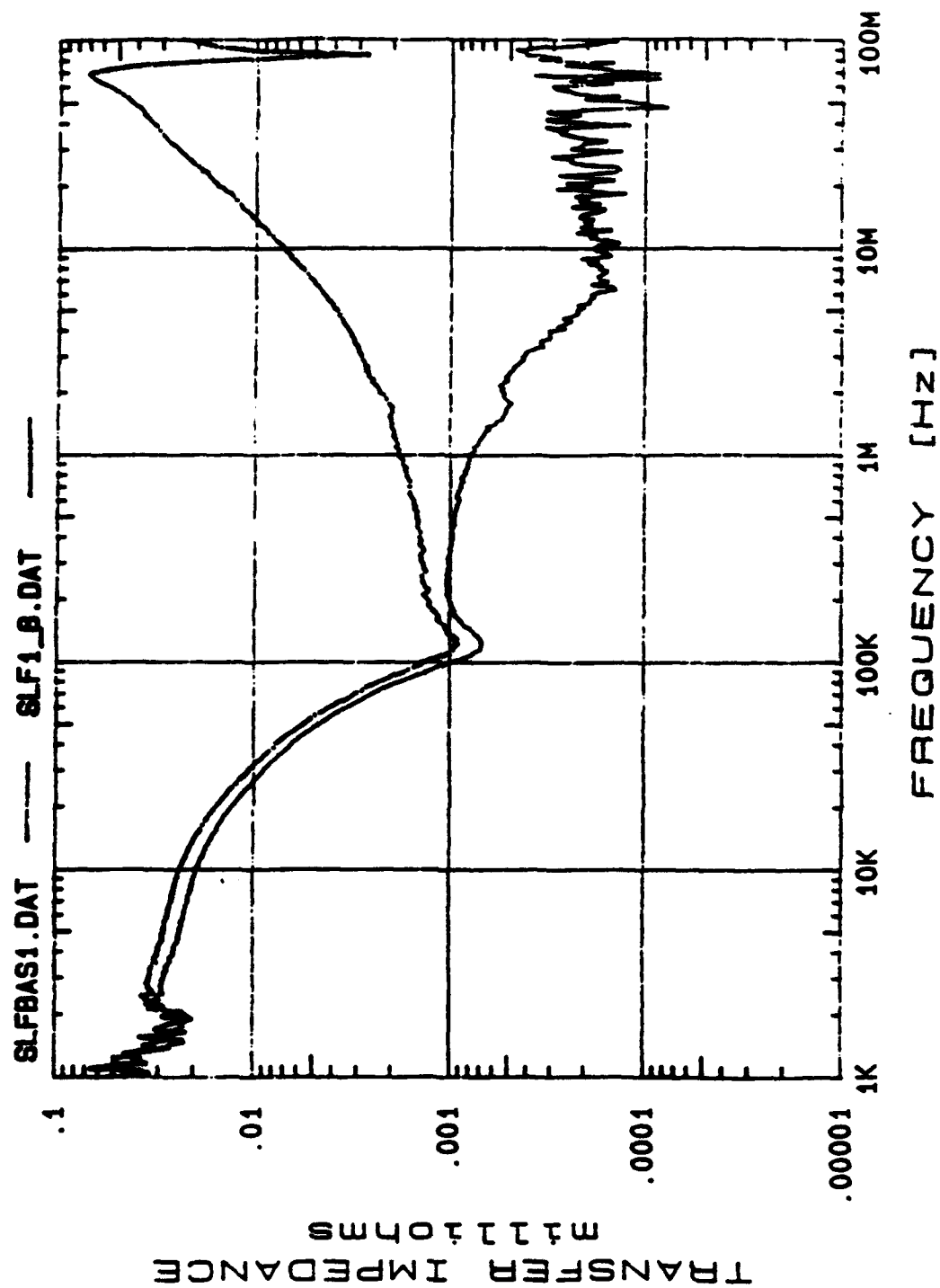
Overlay of the baseline response and of single holes.
1/8", 3/16" and 1/4" diameter.

SLF8AB1D8XT —— SLF3_16.DAT —— SLF1_4.DAT ---
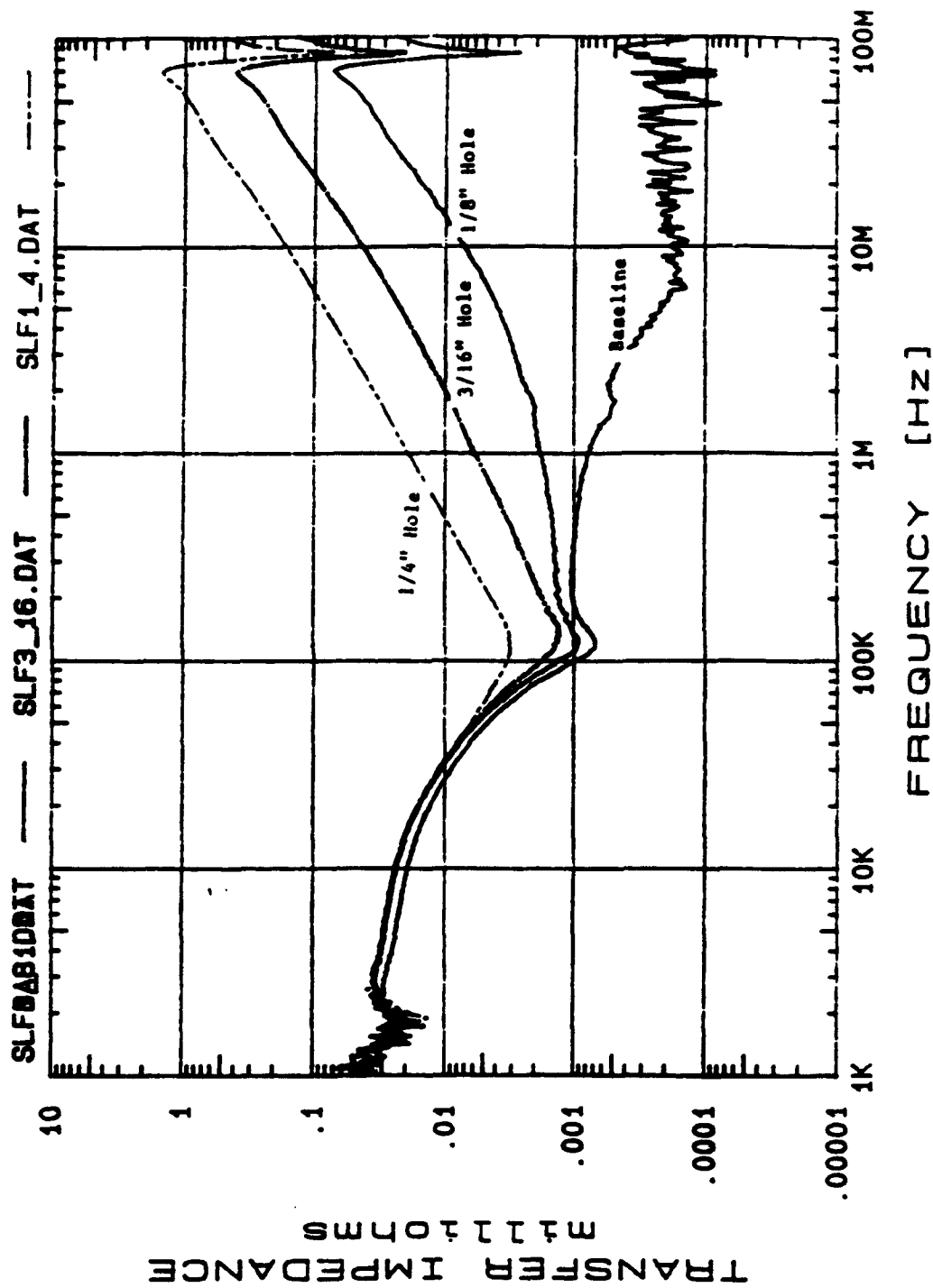
Plot 6

Overlay of the baseline response and the responses with gashes 1" and 2 3/4"

SLFBAS1.DAT ——— SLF16.DAT ——— SLF3G.DAT —·—

Plot 7.